BLADE VIBRATION MEASUREMENT TECHNIQUES

AND

VIBRATION ANALYSIS OF PLATES

BLADE VIBRATION MEASUREMENT TECHNIQUES

AND

VIBRATION ANALYSIS OF PLATES

BY

D.V.JAGANNATH, M.E.(Propulsion)

A Thesis

Submitted to the Faculty of Graduate Studies

in Partial Fulfillment of the Requirements

for the Degree

Master of Engineering

McMaster University

March 1969

MASTER OF ENGINEERING (1969)
(Mechanical Engineering)

McMASTER UNIVERSITY
Hamilton, Ontario.

TITLE: Blade Vibration Measurement Techniques and Vibration Analysis of Plates.

AUTHOR: Jagannath, D.V., M.E. (Propulsion)

SUPERVISOR: Dr. Dokainish, M.A.

NUMBER OF PAGES: viii, 95

SCOPE AND CONTENTS:

Literature on experimental techniques for measurement of gas turbine blade vibration has been reviewed.

First natural frequency of a cantilever plate of thin uniform rectangular cross section, with and without pretwist has been obtained experimentally.

Free vibrations of cantilever plates of thin uniform rectangular cross section have been analysed by Finite Element Method. Computed values of natural frequencies and mode shapes are compared with other analytical results.

ABSTRACT

The present investigation deals with Gas Turbine Blade Vibrations.

Literature on the techniques employed for experimental investigation of gas turbine blade vibration characteristics has been summarised. Various steps have been explained by reviewing the different techniques. Several causes for possible excitation of blades as well as damping methods to suppress the resulting vibrations are also included.

Attempts were made to determine experimentally the natural frequencies of cantilever plates of thin uniform rectangular cross section, with and without pretwist. First natural frequency of the plate without twist was in good agreement with the one calculated from the plate formula.

Free vibration analysis of cantilever plates of thin uniform rectangular cross section is made. Finite Element Technique is used to determine the elastic and inertial properties of a fully compatible triangular element. Computed values of natural frequencies and mode shapes are compared with other analytical results.

ACKNOWLEDGEMENTS

The author expresses his sincere thanks to Dr.M.A.Dokainish, Associate Professor, Mechanical Engineering, for his guidance and encouragement during this research program.

This study was supported by the National Research Council Grant No. A-2726.

NOMENCLATURE

(X,Y,Z)

...Datum Coordinates.

$(\bar{x},\bar{y}),(\bar{\bar{x}},\bar{\bar{y}}),(\bar{\bar{\bar{x}}},\bar{\bar{\bar{y}}})$

... Local coordinates for subtriangles a,b and c respectively.

u_z ... Displacement normal to middle plane of the element.

u_x ... Displacement caused by rotation of normal to the middle plane about x-axis.

u_y ... Displacement caused by rotation of normal to the middle plane about y-axis.

U .... Nodal displacement vector.

$\ddot{U}$ .... Nodal acceleration vector.

e .... Total strain.

ε .... Elastic strain.

e_T ... Thermal strain.

e_I ... Initial strain.

δu_i .. Virtual strain energy.

δw ... Virtual work.

δu ... Virtual displacement.

δe ... Virtual strain.

P .... External force vector.

$[k]_a, [k]_b, [k]_c$

... Stiffness matrices of subtriangles a,b and c in their respective local coordinates.

$[m]_a$, $[m]_b$, $[m]_c$

...Mass matrices of subtriangles a,b and c in their respective local coordinates.

$[k]_L$ ..Stiffness matrix in local coordinates of the set of three subtriangles.

$[m]_L$ ..Mass matrix in local coordinates of the set of three subtriangles.

α .....Column vector of 27 local coordinates.

$[A]^{-1}$ ..Transformation matrix of size 27x9 relating the 27 local coordinates to the 9 nodal displacements of the complete triangle.

$[\bar{k}]$... Stiffness matrix of the complete triangle in datum coordinates.

$[\bar{m}]$... Mass matrix of the complete triangle in datum coordinates.

$[K]$... Condensed stiffness matrix for the entire structure.

$[M]$... Condensed mass matrix for the entire structure.

E .... Young's Modulus, lb_f/in^2.

ν .... Poisson's ratio.

ρ .... Weight density, lb_f/in^3.

ℓ .... Plate length, in.

t .... Plate thickness, in.

ω_n ... Natural frequency of undamped free vibrations, radians/sec.

β .... Natural frequency in non-dimensional form.

q .... Column vector of amplitudes of displacements U.

CONTENTS

1. INTRODUCTION

Mechanical structures are subjected to vibrations due to the presence of periodic or non-periodic forces acting on them. The severity of vibration depends on the magnitude and frequency of these forces.

In the aircraft and missile field, these forces are caused internally in engines as well as by air stream turbulence. A critical review of various problems with present day jet aircraft reveals that those associated with blades emerge high in order of importance. A Bristol Siddely engineer said, "It is not surprising when it is realised that there are some 2000 fixed and rotating blades in an axial engine and the failure of any one of them can cause it to be shut down in flight and score a black mark for an unscheduled removal".

Gas turbine blades can fail if they are subjected to alternating forces having frequencies, near their resonant frequencies. The danger of blade resonance and consequential failure due to fatigue is too well known to require amplification. If the natural frequency of the blade is outside the operating frequency range of the machine and does not coincide with the harmonic speeds, fatigue failure due to blade vibration could be avoided by a suitable choice of design.

Thus a need has arisen for practical determination of the natural modes of vibrations of blades. But since the natural frequencies of blades of the same row in some turbines have shown up to 20% scatter, and with different blade shapes in succeeding rows, complete avoidance of resonance is a remote possibility and necessitates studies on damping and use of dampers.

The blade engineer is interested in the data of natural frequencies and vibratory stresses, when the turbine blades are performing in their normal environment. Experimental results are not completely satisfactory due to tremendous problems while simulating the actual conditions, in the laboratories. Flight tests also exhibit problems due to inaccessibility. There are, no doubt, certain limitations in analytical methods, while making basic assumptions corelating the boundary conditions and the system of disturbing forces. As a compromise, perhaps, it is usual practice to investigate the problem experimentally as well as analytically to achieve some satisfaction, if at all the two results are in fair agreement.

2. LITERATURE SURVEY

2.1 Experimental Techniques

Consistant research has been carried out for more than two decades in the field of turbine blade vibration by engineers all over the world including leading aircraft companies like Rolls-Royce, Bristol Siddely, Pratt and Whittney and so on. Various experimental techniques have been developed and theoritical investigations carried out.

The importance of experimentation for determining blade vibration and fatigue properties can be pointed out by stating that the analytical methods based on theoritical behaviour of the blade, are limited because of unknowns in:

(a) The boundary (mounting) conditions

(b) Aerodynamic stimuli

(c) Blade quality (materials, tolerance variations etc.)

(d) Blade vibratory response to aerodynamic or mechanical excitation and their magnitudes.

The exact mathematical prediction of all natural frequencies of a given blade of an aerofoil section with twist and taper is rather a difficult matter. But approximate methods making simplifying assumptions either in the derivation or in the solutions of the mathematical equations, have been suggested for practical purposes. Uncoupled flexural frequencies have been calculated using Timoshinko equations and extension of Myklestead's method, applying corrections for shear, rotary inertia, taper and twist. For calculating the torsional frequencies, Timoshinko and Holzer's methods have been employed. The effect of twist on torsional rigidity has been neglected, but correction for increased stiffness has been applied.

The blade vibration problem consists of finding natural frequencies and nodal patterns of flexural vibration, torsional vibration, coupled modes, effect of disc vibration and elasticity of attachment, effect of damping, causes and nature of periodic excitation and the vibratory stresses and fatigue endurance.

The most desirable experimental data of natural frequencies and vibratory stresses would be the data which are obtained when the turbine blades are performing in their normal environment. These ideal experimental data are extremely difficult to obtain due to inaccessibility. Telemetry and airborne equipments have been developed. They all have merits as well as demerits, in addition, they are not always feasible. Therefore, environments have been developed which will provide realistic experimental data for specific turbine blade structures. These environments are expected to provide the best simulating conditions.

A rotating test loses its attractiveness since it is only possible to simulate:

(a) The centrifugal effect on blade natural frequency

(b) The blade attachment centrifugal load

(c) The temperature effects.

But it is not possible to simulate:

(a) The exact aerodynamic and mechanical excitation

(b) The normal vibratory and bending stresses due to gas forces imposed on the blades.

The basic disadvantages of a nonrotating blade test facility are, the inability to simulate the centrifugal and exciting force fields. A centrifugal field correction factor can be applied to the high fundamental frequency blades. It has been analytically and experimentally shown that this correction is negligible for short stiff blades.

Though an enormous amount of work has been done on rotating as well as nonrotating blades in various types of applications, namely, steam turbines, turbochargers and gas turbines, as problems of more complex nature are being discovered in present day jet powered aircraft, sophisticated methods of assessing blade vibration characteristics are still underway. Hence the need for emphasis on further gas turbine blade vibration study in the laboratory.

Any blade vibration rig would consist of a mounting device, an exciter and appropriate instrumentation for observation and analysis, which normally consists of a transducer, signal conditioners, cathode ray oscilloscopes, recorders, analysers, the specifications of each one of these depending on the test requirements (1).*

2.1.1 Blade mounting devices.

Carnegie (2) developed a dynamically isolated vibration test rig by mounting the blade on a very heavy clamping block resting on a sponge rubber to make the natural frequency of the block/sponge system low relative to that of the blade, so that the transmitted force (from blade to mounting) is only a small fraction of the impressed force (on the blade)- vibration isolation theory. During rotating blade tests, conventional turbine discs have been used, which completely eliminate errors due to blade mounting.

Earlier parts of the work (3) consisted of some crude experiments with the blade fixed on a swage block. Based on the results of these experiments, a blade mounting rig was developed. The block that holds the blade root can be of any shape to suit the root. The whole mounting was sufficiently heavy and rigid to comply with the assumption of fixed end of the cantilever blade in

* Numbers in brackets designate References.

the theoritical calculations.

Thomas Vuksta (4) gave an experimental curve, showing the effect of base mass to cantilever mass ratio on the fundamental frequencies of cantilevers. See Figure 1. He concluded that the fixture system has to be versatile to permit installation and removal of blades with a minimum effort and it had to be rather massive to permit vibration studies of heavy, high fundamental frequency blades. In order to minimise the physical size of the fixture and fixture-blade mass effect, a 2000 lb. steel block was selected and for this fixture, a blade or blades weighing up to 20 lbs. could be vibrated with a possible error of 0.5% at a mass ratio of 100 to 1. An acceptable error of 1%would permit the blades weighing approximately 25 lbs. to be vibrated in the fixture. Also during blade rig fatigue tests carried out by Armstrong (5) the blade root was rigidly clamped in a massive steel block.

2.1.2 Excitation methods.

Various techniques have been adopted in laboratories to vibrate or fatigue the blades.

Excitation by bowing is quite obselete- the blade is set in vibration by drawing a bow, such as a violin bow, across the blade root. Complex modes cannot be excited this way.

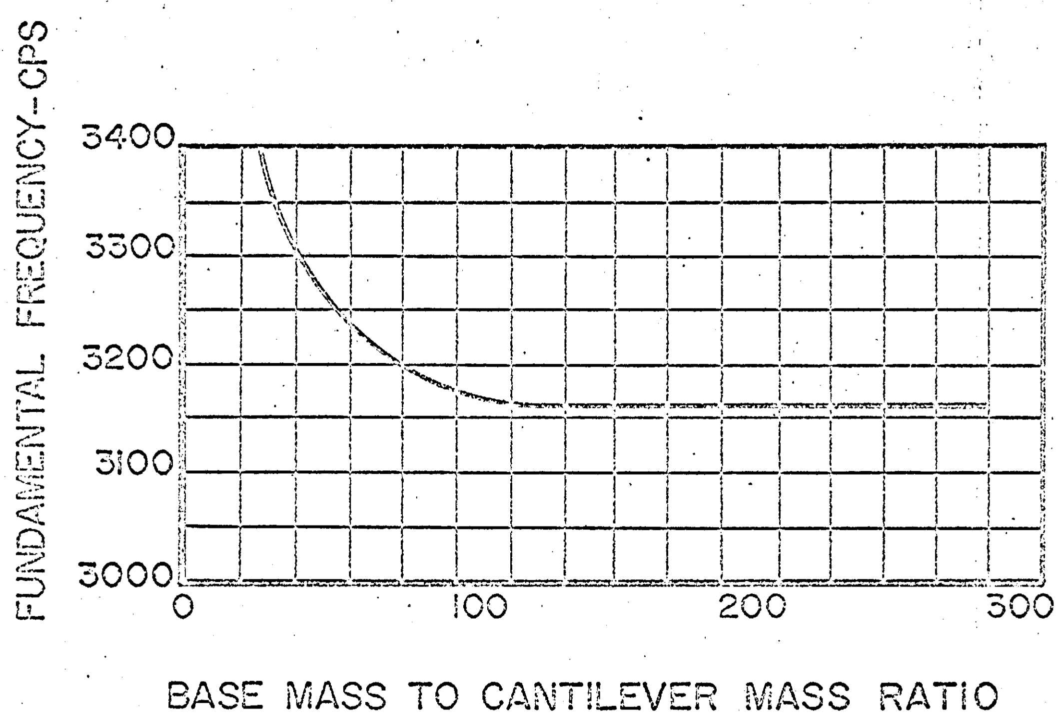
FUNDAMENTAL FREQUENCY-CPS
3400
3300
3200
3100
3000
0
100
200
300
BASE MASS TO CANTILEVER MASS RATIO

FIG. I

Acoustic excitation employs a low voltage sonic driver to direct sound energy through a truncated cone to a localised area of the blade. This is limited due to absorption of sound energy in the surroundings and low power output.

Electrostatic excitation forms the blade as one of the electrodes of a condenser, the other electrode being a stiff piece of metal (e.g.brass), the lowest natural frequency of which(6) is above the range being investigated. An alternating voltage of about 5000 V between the two electrodes placed 1/10" apart causes the blade to vibrate and enables resonances to be detected. The exciting voltage is produced by feeding a variable frequency signal from an audio-oscillator through a 25 watt amplifier and step up transformer. This is seldom used in laboratories because of low power output.

Pneumatic excitation directs high velocity air stream from a nozzle towards the blade tip and by suitably adjusting the distance between nozzle and the blade successfully excites modes up to 2000 cps. Mechanical difficulties arise while exciting higher modes. To overcome these difficulties, pulsed air vibration techniques have been employed. Air is passed through a slotted rotating wheel which is close to a stationary plate having identical openings. This alternate opening and closing of the duct produces pulsations in the air and the frequency of pulsations is proportional to the speed of rotation and the number of slots. The vibration amplitude is controlled by a valve on the air supply line. The facility is also capable of elevated temperature operation by heating the excitation air with a direct fired heater using JP_4 fuel (7). This technique of pulsed air vibration has been successfully used by Truman, Martin and Klint (8) up to frequencies of 15000 cps, for higher mode fatigue failures, both flexural and torsional.

Blade resonant frequencies have been produced by mechanical excitation, using vibration shaker tables, magnetostrictive metal bars and crystal type transducers. The drawback is that the stress distribution is affected and at higher frequencies, this force is not sufficient to carry out fatigue tests(9).

An overall survey of exciters working on the electromagnetic principle includes systems working on

(a) Eddy current principle (permanent magnet type and D.C. electromagnet type)

(b) Half wave rectifier principle (solenoid type and "U" shaped electomagnet type).

Though the permanent magnet type is generally employed for blade vibration studies in aircraft industries, it has got its limitations for effecting peak starting pull at high resonant frequencies.

This rig is used for magnetic blades and if the blade is of nonmagnetic material, a soft iron piece is installed at the blade tip. The A.C. flux in the core alternates at the set frequency of the oscillator and induces voltage on the blade surface. Since the available power output is limited, this system is unsuitable for vibrating very stiff blades(10).

High starting force can be achieved by taking advantage of the increased field in case of a D.C. electromagnet. Since D.C. and A.C. flux paths are isolated except at the pole tips (where suitable holes or slots are to be made to avoid transformer action by cutting of fluxes) this method can be successfully used to vibrate heavy nonmagnetic blades. See Figure 2.

Bench fatigue tests carried out by Voysey (11)on turbine blades by an electromagnetic exciter consisting of a moving coil speaker indicated a pull of ±180 lbs. at the moving coil with 1000 watts input, due to interaction of A.C. in the coil with the steady field of a 400 lb. D.C. magnet. This system could be used satisfactorily up to 3000 cps.

Electromagnetic exciters working on half-wave rectifier principle, developed by Canadian Pratt and Whittney (10), that are capable of producing starting pulls of the order of 400 lbs. or more, can vibrate the blades at resonant frequencies of sevaral

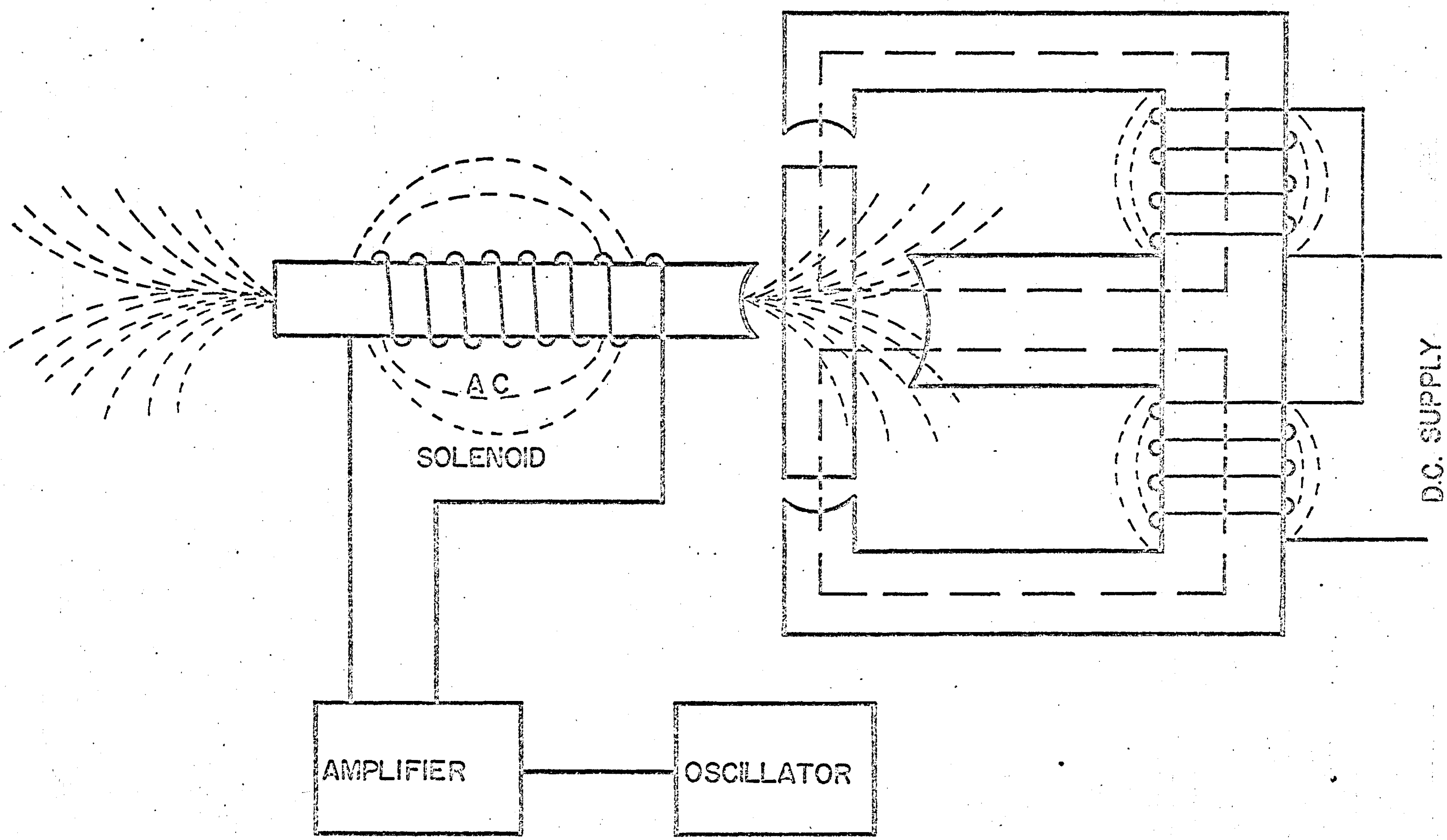

FIG. 2 FLUX PATH OF EDDY CURRENT RIG.
(D.C. ELECTRO MAGNET TYPE)

kilocycles and with a maximum amplitude of 0.5" or more.

Half cycle voltage waves are applied to two solenoids through rectfiers. The power is fed from a power amplifier driven by an oscillator. The circuit capacitance is varied to decrease the line current at the resonant frequency of the blade. The vibrating head consists of transformer laminations which are stacked inside two ebonite channel pieces. These are held rigidly to the blade tip by a barrel nut and the space around the blade tip between the ebonite channels is filled with plastic cement. These exciters working on half wave rectifier principle have been successfully used to perform studies of nodal patterns and fatigue failures, both flexural and torsional, of different types of blades and vanes.

2.1.3 Instrumentation.

Each detail of operation must be given careful attention in order to successfully measure turbine blade vibrations. As an example, in case of a turbocharger operating at speeds as high as 100,000 rpm, blades vibrate at frequencies greater than 20,000 cps, when the turbine wheel is operating in the exhaust gases at temperatures up to 1,400 deg. F. Under these conditions, signals are to be produced and transmitted to recording equipment that will faithfully record the events as they occur(12).

The first component in the instrumentation circuit of any vibration test rig is the vibration pick up (detector). Depending on the type of pick up used, its output can be used to measure vibration amplitudes, stress distribution and visualise the actual phenomenon on a cathode ray oscilloscope screen and then the various mode shapes could be traced.

Detectors:

In most rotating blade tests, strain gages have been used for strain measurements and to pick up vibrations. Bristol Siddely in 1962 have developed frequency modulated grid technique and radio frequency methods.

In the frequency modulated grid system, a zig zag conductor in the stator casing and a magnet at a rotor blade tip generate a series of electrical impulses at a constant frequency. If the blade is vibrating, the frequency of the impulses will fluctuate and the signal is proportional to the component of the blade alternating velocity at right angles to the bars of the conductors. Blade calibration in the relevent modes to relate the measurement to that of the standard position of the leading edge, allows the result to be given in terms of (a x f), where f is the frequency and a is the leading edge tip amplitude. The factor (a x f) is a direct function of maximum stress. The radio frequency method employs a high frequency signal (475 kc/s- Bristol Siddely) which is transferred to the rotor by an inductive slip ring. This signal supplies the D.C. polarisation current for the gages. The gage signal is amplified and then frequency multiplied with gage signals from other channels prior to being transmitted to the stator through a single capacitive coupling ring.

In case of nonrotating blade tests, the types of pick ups used, other than resistance wire strain gages, (the type of gage depended on the range of temperatures and various forces on them- for e.g.- during a rotating test, centrifugal force on the gage was 40,000 times the weight of the gage), are of crystal type, acoustic type, capacitor type and the optical type.

Barium titanate and lead zerconite have exhibited much better piezoelectric properties than quartz and rochelle salt and hence have been used as detectors as well as exciters in vibration studies. Ferroelectric ceramics such as barium titanate (sensitivity $=0.1$ v/10^{-6} unit of strain= a few thousand times that of a typical wire resistance gage) are piezoelectric after polarisation in an electric field and have very high dielectric constants, a few hundred times that of quartz, but this property is temperature dependant. At a certain critical temperature, usually about 100 deg. centigrade, they disappear completely and hence need repolarisation at a lower temperature.

Blade vibration has been detected (2) by lightly placing the needle of a piezoelectric gramaphone pick up near the junction of the blade and its root. The output from the pick up is then fed to a voltage amplifier. The limitation is the pick up sensitivity at higher frequencies. This has been employed to make a traverse on the vibrating blade surface, while tracing the nodal patterns(22).

Capacitance type pick up, a noncontacting type of vibration detector has been successfully used to trace the nodal patterns and measure amplitudes.

Brittle lacquers to detect maximum stress regions and a type of sand to visualise nodal patterns have been used. The optical method of detecting blade vibration is carried out by illuminating the vibrating blade with a stroboscope flash and using a microscope to determine the dynamic reflection curves.

A noncontacting electro-optical instrument that has been very recently developed by "Physitech-Inc-Pa., U.S.A." produces electric signals that may be recorded so as to measure vibratory movements including angular vibrations, fast, slow, big or small. It uses a special photomultiplier tube to electronically serve as an optical discontinuity.(13).

Detector location and orientation:

One very important aspect to be considered while using a wire resistance gage is its location and orientation w.r.t. blade.

Other types of detectors do not pose much of problem in this regard.

During stress distribution studies, a number of gages should be necessary. As many as 16 gages have been used on a single blade. But during a fatigue test, one is naturally interested in the point of maximum stress.

Due to the complicated shape of a turbine blade, especially around the root section, it is not possible to locate the gage at the point of maximum stress of a particular mode. Thus the gage signal must be calibrated in terms which can be related to the fatigue strength of the material. By choosing a gage position where the signal is approximately equal for amplitudes of vibration of the same severity (a x f value) in the four modes, it will be easier to observe the amplitudes associated with each mode. But this required that the gages be calibrated for each mode. It is not advisable to mount the strain gage at the point of maximum stress as this may result in premature fatigue failure of the gages themselves.

The blade vibration philosophy (14) developed by Bristol Siddely gets rid of these gage location problems while determining the maximum stress. Vibration has been specified in terms of the total leading edge tip amplitude 'a' times the frequency of vibration 'f', since (a x f) is a direct function of maximum stress for all flexural modes of a uniform cantilever beam.

$$\sigma_{max} = \text{constant x (axf)}$$

Once an alternative position is chosen, some form of calibration (static rig) is done so that the test gage can be related to the blade tip amplitude as easily as the output from another strain gage. Static calibration is done with a microscope fitted with a graticule focussed on the leading edge tip.

In selecting the gage position, one should find a position where the output signal in the number of modes under consideration is of similar level per unit (a x f) and that this signal is large enough compared with the electrical noise levels of the circuits. This facilitates the monitoring of the amplitudes during tests and also the detailed analysis of the test recordings.

During engine tests, amplitudes (a x f values) have been predicted analytically by a thorough analysis of the air intake characteristics, intake distortion and downstream obstructions, involving three computer programs.The spanwise location of the maximum stress being a function of the mode of vibration, one needs to choose a spanwise gage location, in which the local stress is an appreciable fraction of the maximum. The following table gives the third flexural mode stress distribution for standstill and for top speed in a blade of actual interest. (The results have been obtained by numerical methods with an I.B.M. computer (15).)

Table 1

Gage Location % Span	Max. Stress/Local Stress(gage) Standstill	Top Speed
0	1.42	1.00
5	1.96	1.44
10	3.19	2.33
20	8.88	33.30

Other factors on which the optimum gage location depended are

(a) Probable sources of excitation and their relative severity

(b) Blade dynamic response characteristics

(c) Angular location of gages to detect for all conditions, the highest fraction possible of the local stresses and

(d) Strain gage survival.

When the angular orientation θ =90 deg. one may observe full bending strain and fail to read torsion in this idealization, neglecting the end effects and coupling. See Figure 3. A gage reading maximum torsion may read only 1/3 of maximum bending. A gage located at 65 deg. reads approximately 75% of maximum for both bending and torsion.

Fatigue tests have shown that (a x f) depends on the material. Typical values for 10^7 reversals are Aluminium, 5.5 fps, Steel, 6.5 fps, Titanium, 11 fps and Glass fibre laminates, 13 fps.

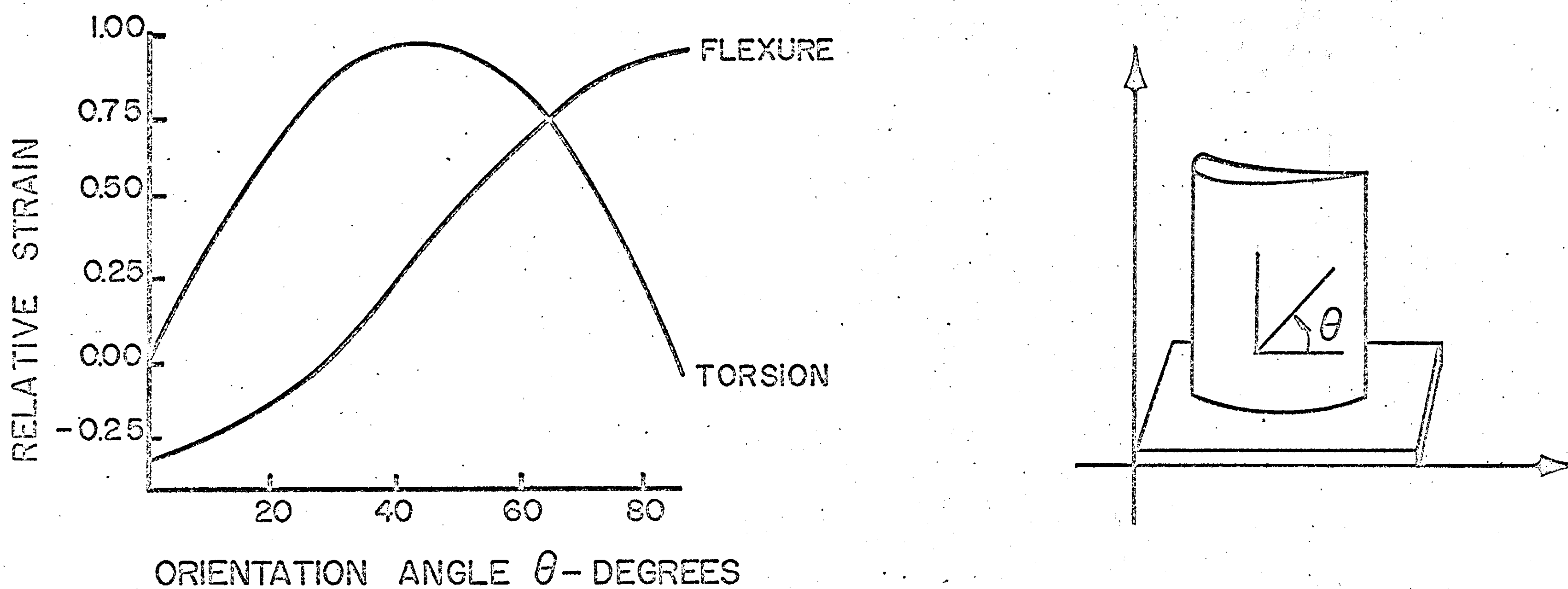
RELATIVE STRAIN
1.00
0.75
0.50
0.25
0.00
-0.25
FLEXURE
TORSION
20
40
60
80
ORIENTATION ANGLE θ - DEGREES
θ

FIG. 3

For design purposes if (a x f) exceeds 2 fps, amplitudes of vibration are considered to be serious (19).

The severity of vibration has then been specified by a parameter "Amplitude Ratio" given by

$$\text{Amplitude Ratio} = \frac{\text{measured amplitude (a x f)}}{\text{failing amplitude (a x f) for 100 hour fatigue life}}$$

Fatigue test starts with (a x f) = ±5 fps vibrated for 30 minutes at this level, before increasing the (a x f) value by ±0.5 fps for another 30 minutes and continues this way until failure occurs.

If the amplitude ratio is greater than 100%, adequate engine restrictions must be imposed until satiafactory modifications have been incorporated.

If it is between 50 and 100%, failure during long service use is expected and long term remedial measures are to be taken.

If the amplitude ratio is less than 50%, the vibration may be considered to be not serious for full service use.

Signal transmission:

When carrying out strain gage tests, it is usual practice to observe initially the signals from few blades per stage, the limiting factors being the slip ring and recorder capacities. During the analysis, however, and subsequent testing of the engine, only the signals from the two blades showing the largest amplitudes are transmitted. Nonrotating tests are not too troublesome while transmitting, since direct connections are possible.

Rotating tests have incorporated several types of devices for successful transmission of signals from the rotating parts. Brush type slip rings, mercury slip rings and radio telemetry have been used on a variety of tests.

Motsinger reviewed slip ring instrumentation and compiled an extensive bibliography of tests relating to this subject, in his paper "Rotating Instrumentation, a discussion and review of slip ring instrumentation and design". Brush type slip rings are operating up to 100,000 rpm. They generate noise in the signal, at high speeds due to changes in the contact resistance between the brush and the ring. Some employ as many as four slip ring channels for a single information channel(16).

Mercury type slip rings transmit signals at a lower noise level. They have gained more attraction because they require only two slip ring channels for each information channel, since this reduces the overall size requirements and increases the speed capabilities.

Radio telemetry has been successfully employed, mainly during flight tests (17), since this technique is not essential during ground tests.

Signal conditioning, Recording and Analysis:

The output from the detector has got to be conditioned, e.g. the resistance change of the strain gage should be converted to a voltage level suitable for observation of the vibration phenomenon on the CRO screen, as well as for recording on the magnetic tape.

The size of the equipment for signal conditioning, recording and analysis depends on the type of test, e.g., the instruments required for a multistage compressor test must necessarily contain a high number of channels, yet be efficient and reliable in operation.

A system employed at the General Electric Company, Ohio(15), included:

(a) Acceptance of 60 input signals simultaneously from a wide variety of detectors

(b) Simultaneous oscilloscope presentation ang magnetic tape recording of any 6 signals in any combination desired

(c) Six channels for recording the wave form on direct writing oscillographs

(d) Auxiliary equipment necessary for operation such as amplifiers, power supplies, etc. built in as an integral part of the system, with strict adherence to the shieling and grounding procedures established for the project.

Recording may be done on multichannel magnetic tape recorders capable of receiving A.M. or F.M. signals. In order to make an automatic waveform analysis, the signal is made repetitive by selecting a length of the tape and making a continuous loop which can be played into an automatic recording wave analyser (18). Tests of this nature have accurately indicated the frequency and amplitudes of blade vibrations and therefore will be valuable in providing results which are directly comparable with those obtained by the manufacturers during production. An electronic wave analyser requiring a frequency setting makes possible direct reading of amplitude of a steady state signal with accuracy straight from the meter provided in the unit(19).

The tape record could be analysed by replaying the tape at a reduced speed into a medium speed camera, but this involves a considerable amount of films. A continuous film camera used by Rolls Royce could investigate only first and second modes. As another alternative, data acquisition systems may be used which record analog information in digital form. To present the recorded information in its most useful medium, choice of output recording devices are available. If the data is to be analysed by a computer, it may be recorded on paper tape, punched cards or digital magnetic tape, as appropriate.

Observation:

Cathode ray oscilloscopes have been used in most cases for visual observation of a vibration phenomenon. Blade natural frequencies, which are directly read on the calibrated dials of variable frequency generators, are easily detected by bringing the blades to resonance. By suitable calibration, the magnitudes of vibration amplitudes are also measured directly on the CRO screen.

Grinstead (20) reviewed the work of Chladni (1787), originator of the sand pattern for rendering visible the different vibratory motions of a resonant plate. Chladni obtained 52 mode shapes for a square plate, 43 for a circular, 30 for a hexagonal, 52 for a rectangular, 26 for an elliptical, 15 for a semicircular and 25 for a triangular plate. Grinstead demonstrated that complex nodal patterns obtained on turbine blades and impellers vibrating at various modes, derive from consistent series of simpler modes and that the frequencies of the latter, may be plotted in families of curves, and thus has resolved them into their basic modes.

Observations have also been made in the experimental techniques used by Belgaumker (3) that the predominately pure modes could be obtained clearly by properly selecting the location for exciting the blade.

2.2 Causes of Blade Vibration

The various reasons for excitation in a turbo-jet engine are:

(a) Transmission of mechanical vibration through fixings

(b) Flutter excitation

(c) Fixed wake excitation

(d) Rotating stall cell excitation

(e) Random type of excitation.

The class of vibration and excitation mechanisms have been studied(21,22). This leads to a means of reducing the amplitude, by various damping techniques.

Basic experimental work associated with flutter conducted on cascades of blades showed fundamental flexural and or torsional modes, the mechanism of flutter being one of self excitation and is due to the lift characteristics of the blade. Change in angle of attack changes the aerodynamic force on the blade. Force increases for a decrease in angle of attack and then the vibration builds up. A detailed analysis of the strain gage signals has revealed that at moderate amplitudes, the blades vibrate at their own natural frequencies. The peak amplitudes of different blades usually occur at the same speed. Since flutter vibration occurs in either the fundamental flexure or torsional modes, the most responsive section is at the blade tip. A change in rotor tip stagger does, in fact, controls vibration in either mode.

A number of fixed vanes in the annulus of a compressor supporting the bearings are responsible for wakes. The air flow over these vanes create wakes of low air velocity compared to remainder of annulus. Aerodynamic force on the blade rotor is reduced in these zones, the frequency of pulses would be the number of reductions in air velocity times the speed. If this frequency is equal to one of the natural frequencies of the blade, then a fairly large amplitude may build up. Blade vibration caused by wake excitation exhibits all characteristics of a forced resonance. The amplitudes are fairly steady with time for a set speed. Excitation caused due to intake maldistribution may also be included in this category.

During tests, it was found that the air flow at conditions below the stall conditions of the first rotor blade broke up into a series of stalled and unstalled patches (one to eight). The stalled zone rotated in the same direction as the rotor, but at approximately half the engine speed. In these stalled zones where low velocity air exists, aerodynamic force on the rotor blade reduces the stalled zone thus giving rise to a pulsating force as it passes the rotor blade. When these pulsations occur at a blade natural frequency, severe vibrations occur. It has been observed that this type of excitation is non-existant above about 80 percent of the designed speed. Analysis of strain gage signal at any particular speed shows that the amplitude of each mode fluctuates rapidly with time.

In some experiments, the blade vibration present was not caused by any of the above methods, but amplitudes in both flexural and torsional modes were possible. This has been considered to be due to random disturbances in the air flow. This type of excitation is characterised by vibration with time and each blade vibrates at its own natural frequencies. The amplitude distribution of the strain gage signals has been found to posses the character of filtered random noise.

2.3 Damping Methods.

Various damping methods are employed in order to reduce the blade vibration amplitudes. They include:

(a) Internal damping of the blade material

(b) Mechanical damping of the blade fixings

(c) Aerodynamic damping (when a blade vibrates in an air stream it imparts some of its energy to the surrounding air).

Hanson, Meyer and Manson(23) formulated in the following way:

Total damping = Material damping + Aerodynamic damping + Root damping

Material damping was determined by dropping a steel ball in such a manner that it strikes the blade (rotating) near the tip. A plot of log amplitude versus number of cycles is determined, the slope of which gives material damping. Material damping is not enough for high amplitude vibration. Aerodynamic damping cannot take care of flutter vibration, since its source of excitation itself is aerodynamic instability. Total and aerodynamic damping have been separately formulated analytically in terms of the logarthmic decrement. Root damping could then be determined by mere subtraction.

It was found that for tight blades, there is no root damping, regardless of centrifugal force, because the tightness is already induced by the fit rather than by centrifugal force. However, for loosely mounted blades, appreciable damping occurs at low centrifugal forces, but at high centrifugal forces, the root damping falls off essentially to zero, since at higher speeds, it is as good as a tight blade. Root damping of loosely mounted blades depends to some extent on the exciting force at high speeds. Some root damping has been noted through experimental curves. The use of a solid lubricant, such as molybdenum disulphide extended the beneficial effects of looseness to much higher rotative speeds. Hanson developed a pin type damper (24) applicable to axial flow compressor blading which brought down the vibratory stress by a factor of ten. It is based on the principle of sliding friction between contacting metals involving centrifugally loaded pins that contact the blade and the rotor. This means supplemented the inherent damping of the blade system, inherent damping sources being internal friction of the material, dissipation to air, dissipation to blade root and dissipation by mounting. See Figure 4.

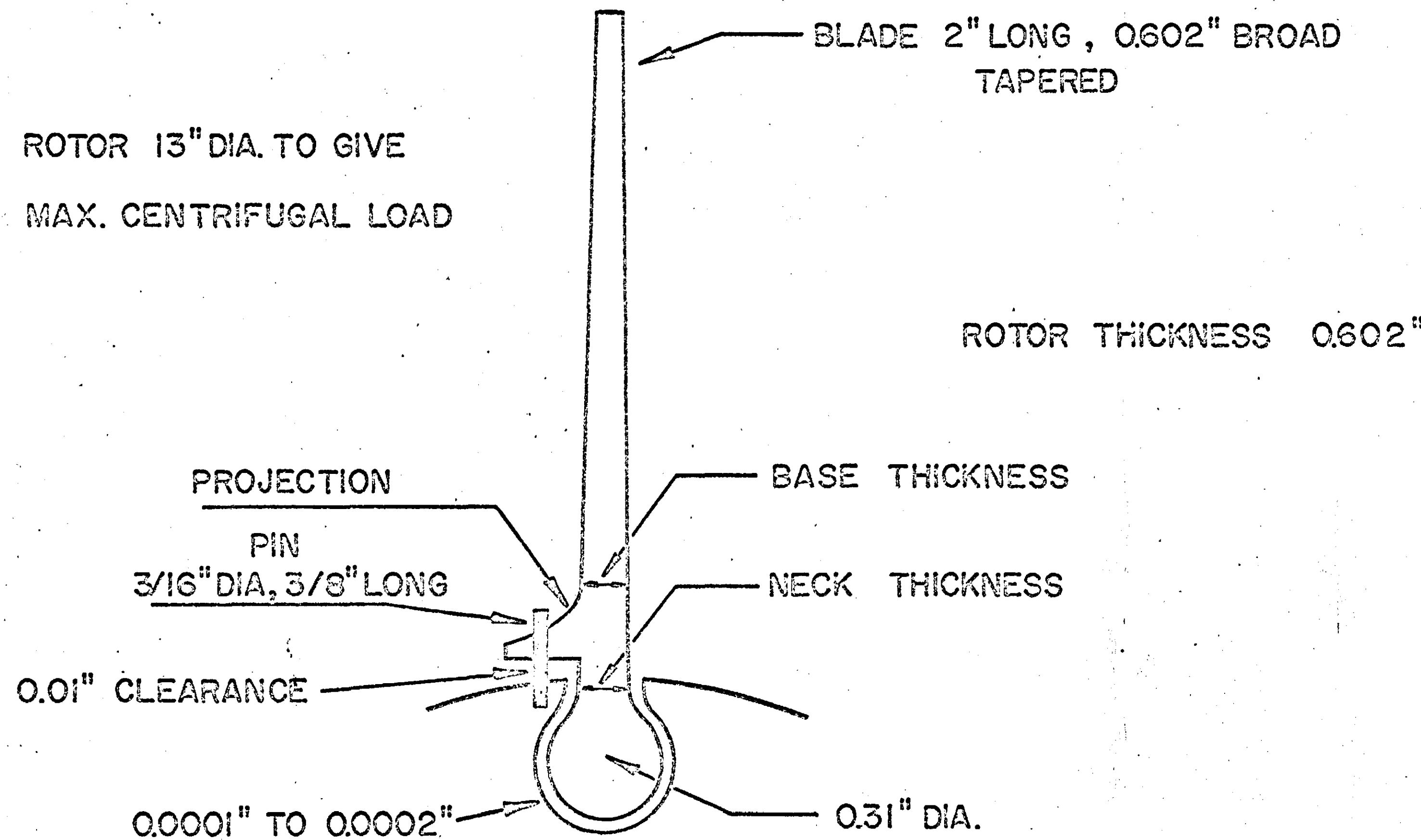

FIG. 4 PIN TYPE VIBRATION DAMPER

Experiments carried out up to 1500 rpm using air jet excitation, strain gages and monel slip rings, helped study the influence of variables such as pin fit and material, blade proportions and damper endurance. No systematic study was made to determine the optimum pin size. Damping seems to be more effective after 20hours of operation due to increasing friction and rate of wear as surface contamination (oil etc.) wears out. The smaller the ratio of neck to base thickness of the blade, the more effective the damper operation would be. Stresses could be reduced to 1/10 value without damper, by using hardened steel pins (0.0015" diametral clearance) and cast inconel blade mounted in an aluminium rotor. Damping induced by the pin damper remained consistently high with only a small effect of centrifugal loading.

The use of wires as a means of damping has been developed (25), for application in various vibratory components including gas turbine blades (vibrating due to flutter and stall) stationary as well as rotating, with a good agreement between test and theory. The method of damping through wires is based on the theory:

(a) In case of stationary blades, the vibration of blades containing damper wires causes a squeezing action resulting in rubbing of the wires, dissipating vibratory energy of the blade.

(b) In case of rotating blades, wires adhere to a wall of the blade due to a centrifugal action and the vibratory motion of the blade causes relative motion between the blade wall and the adjacent wires to absorb energy.

Analytical investigation starts with the calculation of work done between two wires, finding the total work per cycle and then equating it to the change in kinetic energy of the system per cycle, thus obtaining an expression for ratio of the change in tip deflection to the tip deflection ($\Delta y/y$). The logarithmic decrement ($\log(1/1-\Delta y/y)$) which could thus be related to that ratio, is a measure of damping. Experiments have been carried out on a hollow stator vane filled with loosely packed 946 strands of 0.005" diameter copper wires. One end of the vane was welded to a plate, fastened to a large fixed mass to approximate to a cantilever beam and the resulting signal was displayed on the CRO. The blade was excited by hand and the observed decay wave on the CRO screen was photographed by a polaroid land camera.

Tests on rotating blades were conducted at different speeds to change the centrifugal components on the blade and hence their lean angles and with different number of wire strands inside the blade. High speed moving pictures of wires in a vibratory blade (which had its tip open) exposing the ends of the wires, showed the rubbing, squeezing and unsqueezing action of the wires.

It has been suggested that laboratory testing for the effect of wire diameter and material of the wire on damping ability should be carried out.

3. EXPERIMENTAL INVESTIGATION

The basic intention was to determine the natural frequencies of pretwisted plates. It was also decided to conduct experiments on plane cantilever plates in order to establish the effect of pretwist.

Figure 5 shows a schematic diagram of the experimental set up. A 6"x2"x1/16" mild steel plate was chosen for experimental purposes. One end of the plate was fixed to a heavy steel block. This is shown in the overall view of the set up in Figure 5-a. The tip of the cantilever was excited sinusoidally by an A.C. electromagnet, see Figure 6, powered by an amplifier used to amplify the signals from a frequency generator. The amplitude of the exciting force was maintained constant while changing the frequency. This constancy was checked through an ammeter connected in series with the electromagnet.

Resonance was observed on the cathode ray oscilloscope screen by using a proximity transducer of the capacitance type connected through an oscillator and a reactance converter to the oscilloscope. The electronic circuit converts the movement of the vibrating cantilever into voltage signals which are fed to the Y-input of the oscilloscope. The experimental set up did not pose any problem

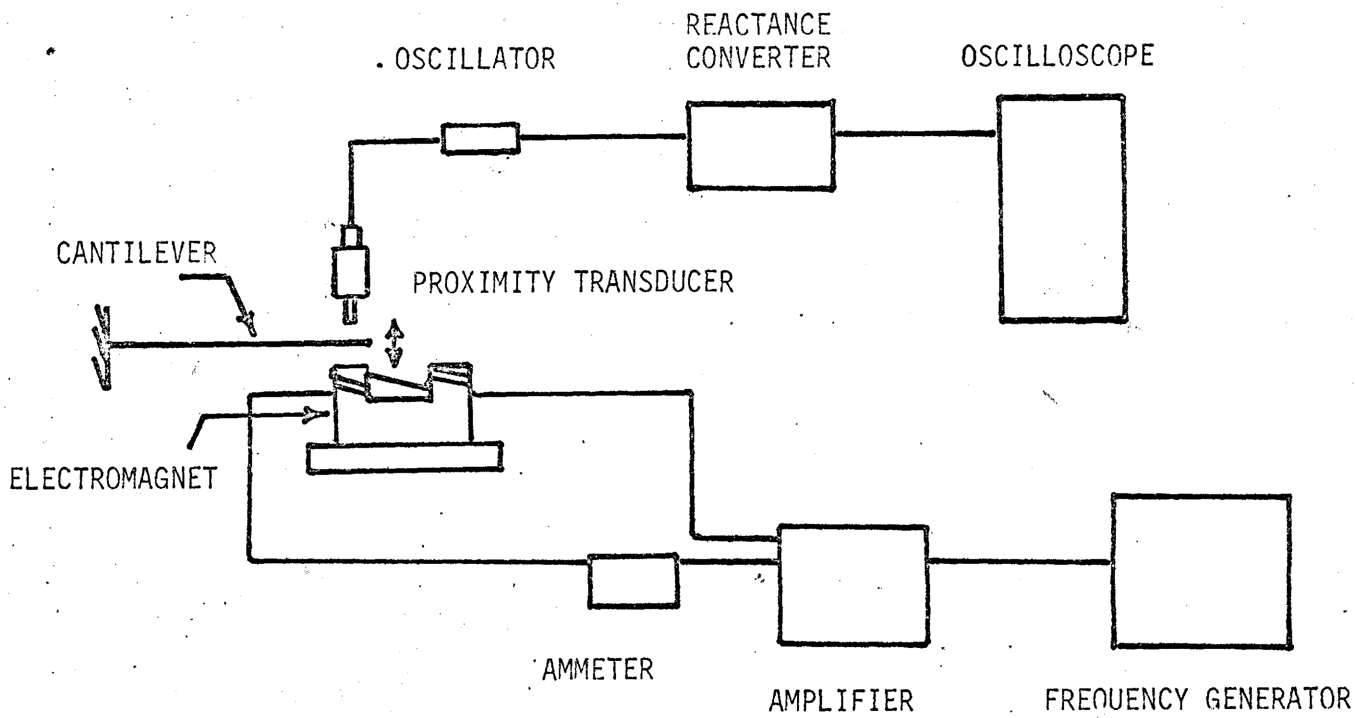

FIG. 5. SCHEMATIC DIAGRAM OF THE EXPERIMENTAL SET UP.

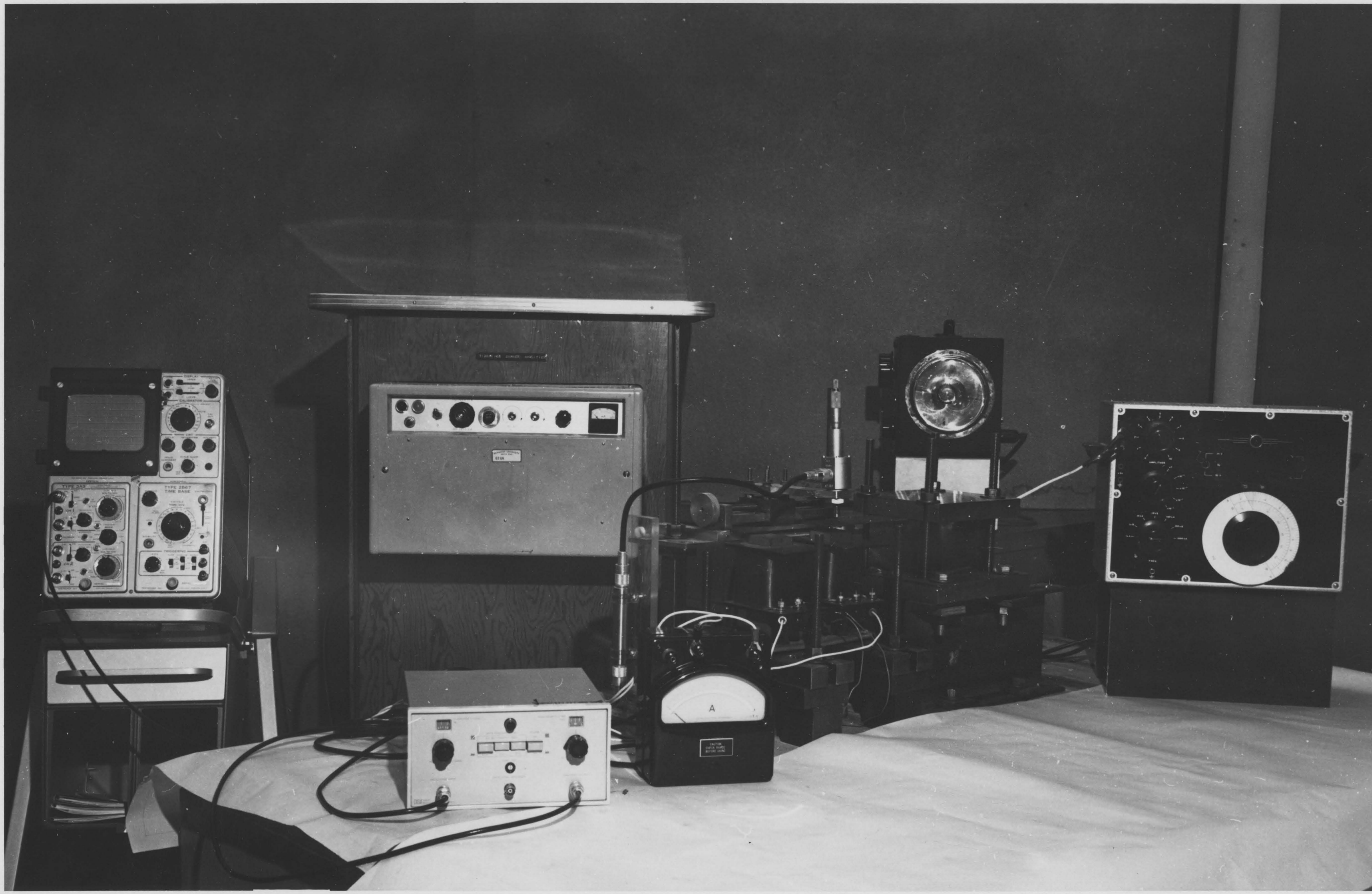

FIG. 5-a. OVERALL VIEW OF THE EXPERIMENTAL SET UP.

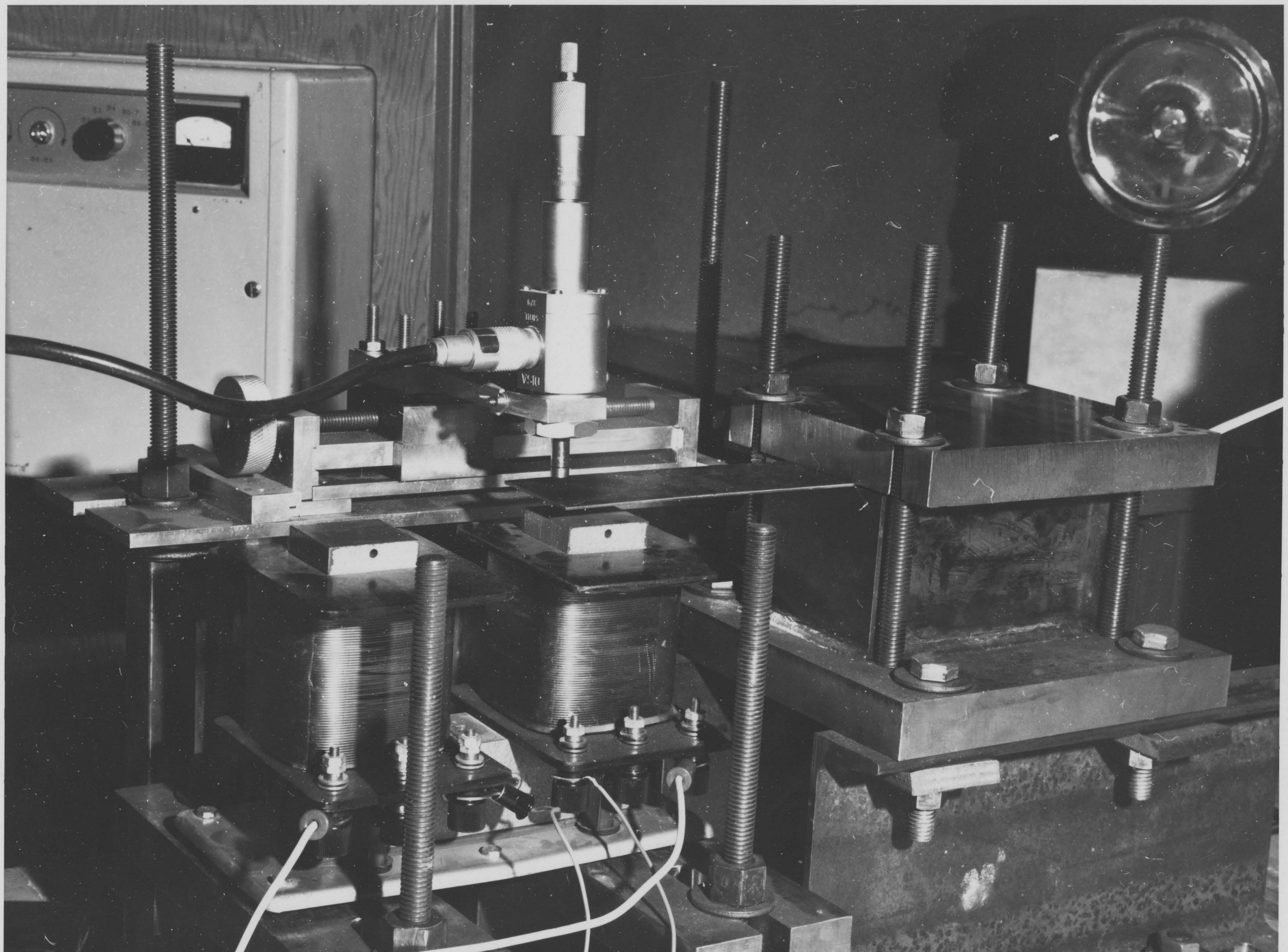

FIG. 6. DETAILS OF EXCITER AND DETECTOR LOCATION.

while determining the first natural frequency. But higher natural frequencies could not be traced. No specific and concrete reasons could be found out for this behaviour of the set up. Similar procedure was carried out for the same plate but with a total pre-twist at the tip of 20 degrees. Twist was provided by using the head stock of a machine shop lathe. The plate was checked for linear variation of twist,(26,27).

The first natural frequency was found to be 54.5 cycles per second for the plane plate and 59.5 cycles per second for the twisted plate. The calculated value from the plate formula (28) for the first natural frequency of the plane plate was 58.54 cycles per second. The plate formula used is:

$$\text{First Natural Frequency} = \frac{3.462}{2\pi}\sqrt{\frac{Dg}{\rho t \ell^4}} \quad \text{cycles per second.}$$

Before chosing the electromagnet for providing the sinusoidal exciting force, a Goodman electromagnetic vibration shaker was used as the force generator. Various configurations, shown in Figure 6-a were attempted while exciting the cantilever, but the values of the natural frequencies so obtained were not reliable.

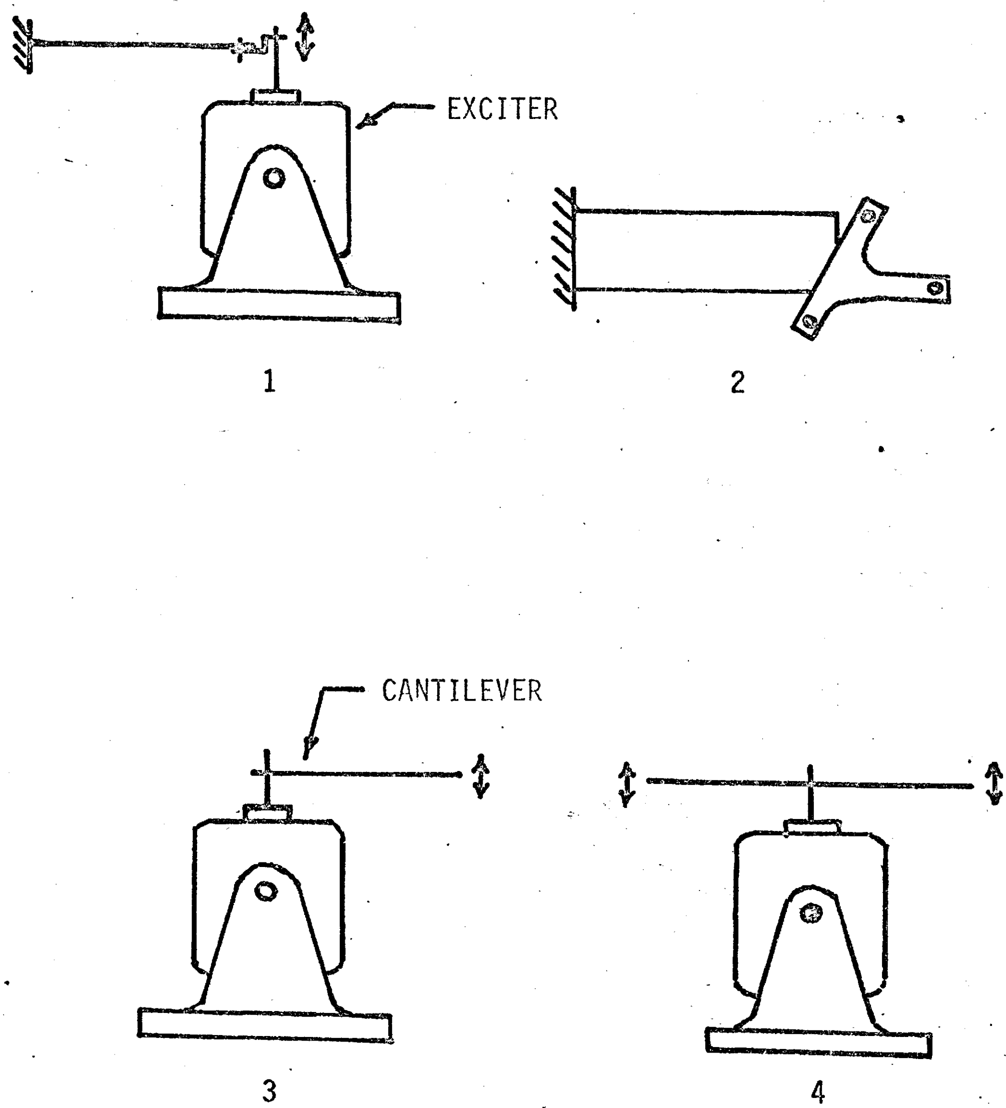

FIG.6-a. CONFIGURATIONS FOR EXCITING THE CANTILEVER.

4. THEORITICAL ANALYSIS

4.1 Introduction

Analysis of complex structural configurations lead to the development of approximate methods, since the conventional methods, although satisfactory when used on simple structures, were found inadequate. Accurate analysis of structural problems is necessary, capable of predicting any stress concentrations so that structural fatigue failures might be avoided. Also speedy computations are necessary to have comprehensive information on the structure, sufficiently enough in the design cycle, so that modifications could be incorporated before taking a decision on the final design. In order to achieve the most efficient design, a large number of different structural configurations may have to be analysed rapidly before a particular configuration is selected.

The method of analysis which meets the above said requirements use matrix algebra which is ideally suited for automatic computation on high-speed digital computers. This is precisely what the "Finite Element Technique" is. This technique has been employed in the present study(29).

The essential feature of the finite element method is the means by which the differential equations of equilibrium of the elastic continuum are approximated by a set of algebraic equations.

The actual continuum is considered as an assemblage of discrete elements, interconnected by a finite number of nodal points. In this method, the digital computer is used not only for the solution of algebraic equations but also for the whole process of structural analysis from the initial input data to the final output which represents stress and force distributions, deflections, influence coefficients, natural frequencies and mode shapes.

4.2 Displacement Function

The most critical factor in the entire finite element analysis is the selection of the element deformation functions. The deformation functions assumed must be able to reproduce distortions actually developed within the continuum. The function used in the present investigation was suggested by T.K.Hsieh. Tocher and Clough (30) used this while deriving the bending stiffness matrix for a triangular element. It reads as follows:

$$u_z = \alpha_1 + \alpha_2 x + \alpha_3 y + \alpha_4 x^2 + \alpha_5 xy + \alpha_6 y^2 + \alpha_7 x^3 + \alpha_8 xy^2 + \alpha_9 y^3 \qquad \text{----(4.1.1)}$$

The first three terms represent the rigid body displacements, without which the laws of statics will be violated. The second three terms represent strain states where as the last three represent variation in strains.We are restricting ourselves to nine constants namely $\alpha_1, \alpha_2, \ldots \alpha_9$, since a maximum of nine constants could be evaluated by means of nine algebraic equations obtained by calculating the nine degrees of freedom present in a triangular element in bending.

The term, a constant times x^2y has been excluded from the cubic polynomial with a purpose. Full slope and deflection compatibility are achieved by dividing the triangular element in question into three subtriangles and suitably chosing the sub-element local coordinate system as shown in Figure 7-b. That is, x-axis in the local coordinate system is always directed parallel to the exterior side of the subelement. Slope compatibility along the exterior boundaries is attributed to the exclusion of the term in x^2y as well as such a selection of the local coodinate system for the subelements. This could be explained easily as follows. Refering to Figure 7-b, for subtriangle a, the displacement function becomes

$$u_z = \alpha_1 + \alpha_2 \bar{x} + \alpha_3 \bar{y} + \alpha_4 \bar{x}^2 + \alpha_5 \bar{x}\bar{y} + \alpha_6 \bar{y}^2$$

$$+ \alpha_7 \bar{x}^3 + \alpha_8 \bar{x}\bar{y}^2 + \alpha_9 \bar{y}^3$$

Normal slope at every point on the exterior boundary kj is $\delta u_z/\delta \bar{y}$.

$$\partial u_z/\partial \bar{y} = \alpha_3 + \alpha_5 \bar{x} + 2 \alpha_6 \bar{y} + 2\alpha_8 \bar{x}\bar{y} + 3 \alpha_9 \bar{y}^2$$

$\bar{y}$ being a constant all along the exterior boundary, slope all along it is linear. It is this condition which ensures slope compatibility.

4.3 Mathematical Model

The mathematical formulation of the problem was done by discretising the structure. This provides with a finite number of degrees of freedom upon which matrix algebra operations could be performed.

Triangular elements are chosen for discretisation. These are applicable to plane as well as shell type of structures. This is because, curved surfaces could be better fitted with a triangular coordinate area rather than with a rectangular coordinate area. Convergence of the finite element procedure was studied using different mesh sizes as shown in Figure 10. A 6 x 6 mesh was chosen for the final analysis of a square cantilever plate. The corresponding results deviated from Dana Young's energy solutions (28) by a maximum of 2.1 percent.

4.4 Analysis

The structure under investigation is a cantilever plate of thin uniform rectangular cross section. It is required to derive the stiffness and mass matrices to determine the dynamic response of the structure. Stiffness and Mass matrices represent respectively the Elastic and Inertial properties of the structure. Stiffness matrix has been derived in this investigation by using the principle of virtual work.

Only translational inertia of the plate is considered while determining the mass matrix, thus neglecting the effects due to rotary inertia. Derivation of stiffness and mass matrices reduces the problem to one of finding out the eigenvalues and eigenvectors which represent the natural frequencies and mode shapes of the structure.

Every triangular element is first divided into three subtriangles a b and c as shown in Figure 7-a. The elastic and inertial properties of each subtriangle are determined separately in the respective local coordinate system 7-b. While attaching every set of three subtriangles to form the complete element, compatibility is achieved of nodal displacements among the subtriangles at the three vertices and the centroid of the complete element. Also the compatibility of normal slopes at midpoints of the interior edges of the subtriangles is achieved. Slope compatibility is ensured also along the exterior boundaries of every triangular element. This is attributed to the triangularisation of each element and so chosing the local coordinate system that $\bar{x}$-axis for subtriangle a is parallel to the exterior side of a .The properties are then transformed into those in the datum coodinate system. The datum coordinates are shown in Figure 7-a.

Derivation of stiffness and mass matrices for a triangular element in bending is discussed in appendix 1. While assembling the stiffness and mass matrices to obtain the condensed properties

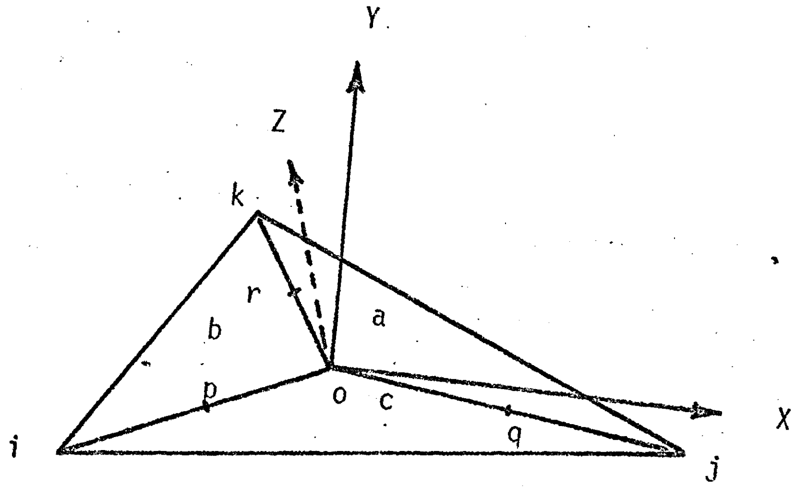

FIG. 7-a. TRIANGULAR ELEMENT IN DATUM COORDINATES X,Y,Z.

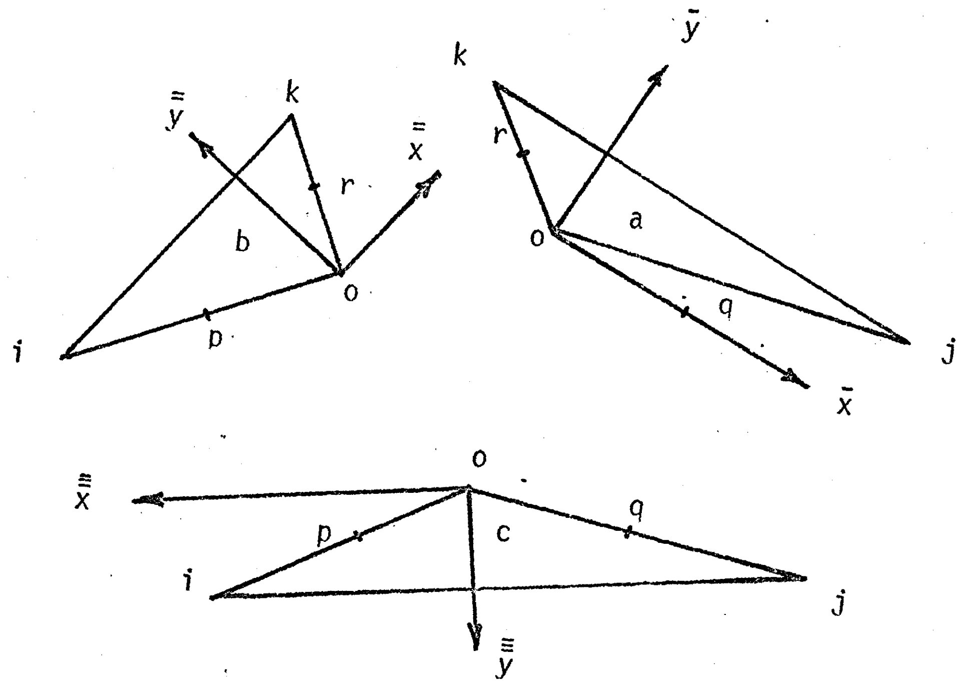

FIG. 7-b. SUBTRIANGLES AND THEIR RESPECTIVE LOCAL COORDINATES.

of the entire structure, the boundary conditions are satisfied for the configuration in question.

The method of determining the condensed matrices for the entire structure could be explained by considering 1x1 mesh for a cantilever, thus discretising it into two triangular elements A and B. The bending stiffness matrix of size 9x9 for each of these triangles could be partitioned into nine units as shown below, each comprising an array of size 3x3.

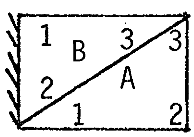

$$A = \left[\begin{array}{c:c:c} A_{11} & A_{12} & A_{13} \\ \hdashline A_{21} & A_{22} & A_{23} \\ \hdashline A_{31} & A_{32} & A_{33} \end{array}\right] \qquad B = \left[\begin{array}{c:c:c} B_{11} & B_{12} & B_{13} \\ \hdashline B_{21} & B_{22} & B_{23} \\ \hdashline B_{31} & B_{32} & B_{33} \end{array}\right]$$

Let us suppose the nodal stations of triangles A and B are numbered anticlockwise as shown. With reference to the entire cantilever, the nodes corresponding to node 1 of triangle A and node 1 of triangle B are inactive since they lie on the fixed boundary. The condensed matrix C of size 6x6 can now be written as

$$C = \left[\begin{array}{c:c} C_{11} & C_{12} \\ \hdashline C_{21} & C_{22} \end{array}\right]$$

where, $C_{11}=A_{22}$, $C_{12}=A_{23}$, $C_{21}=A_{32}$ and $C_{22}=A_{33}+B_{33}$.

Displacement pattern similar to equation (4.1.1) is assumed for each subtriangle.

That is, for subtriangle b,

$$u_z = \alpha_1 + \alpha_2 \bar{\bar{x}} + \alpha_3 \bar{\bar{y}} + \alpha_4 \bar{\bar{x}}^2 + \alpha_5 \bar{\bar{x}}\bar{\bar{y}} + \alpha_6 \bar{\bar{y}}^2$$

$$+ \alpha_7 \bar{\bar{x}}^3 + \alpha_8 \bar{\bar{x}}\bar{\bar{y}}^2 + \alpha_9 \bar{\bar{y}}^3$$

Displacements of the complete triangle involve 27 coordinates α defined by

$$\alpha = \begin{Bmatrix} \alpha_a \\ \alpha_b \\ \alpha_c \end{Bmatrix}$$

where,

$$\alpha_a = \alpha_1 , \alpha_2 , \ldots\ldots\ldots\ldots \alpha_9$$

$$\alpha_b = \alpha_{10} , \alpha_{11} , \ldots\ldots\ldots\ldots \alpha_{18}$$

and

$$\alpha_c = \alpha_{19} , \alpha_{20} , \ldots\ldots\ldots \alpha_{27}$$

Eighteen of these are employed in satisfying internal compatibility requirements between adjacent subelements and the remaining nine are related to the nine discrete displacements U of the element.

A relation between 27 coordinates and 9 nodal displacements is obtained by using compatibility equations. This relation is helpful in finding the elastic and inertial properties of the complete element in the datum coordinate system (X,Y,Z).

For every node in each subelement, deflections and slopes are determined in the respective local coordinates and then transformed to the datum coordinates. The vector representing deflection and slopes at corner k of subtriangle b is written in the form

$$\begin{Bmatrix} u_z \\ \dfrac{\partial u_z}{\partial y} \\ \dfrac{\partial u_z}{\partial x} \end{Bmatrix} = U_k^b = A_k^b \, \alpha_b \qquad \text{---(4.4.1)}$$

Equation (4.4.1) represents a set of three algebraic equations. Equations similar to (4.4.1) but without superscripts refer to the nodal displacements of the complete element.The slopes at midpoints of the interior edges of every subtriangle are calculated. The normal slope at p of subelement c is written as:

$$(S,n)_p^c = U_p^c = A_p^c \, \alpha_c \qquad \text{---(4.4.2)}$$

Equation (4.4.2) represents only one algebraic equation. Using sets of equations in (4.4.1) and (4.4.2), all the compatibility equations are written in the matrix form as in equation (4.4.3). Equation (4.4.3) represents 27 algebraic equations in matrix form. The first nine state that the nodal displacements in the complete element correspond with the subelement displacements at the appropriate corners. Next fifteen define the equality of nodal displacements in adjacent subelements at the corners i, j, k and o. Last three equations impose slope compatibility along the interior edges of the subelements.

$$\begin{Bmatrix} U_i \\ U_j \\ U_k \\ 0 \\ 0 \\ 0 \\ 0 \\ 0 \\ 0 \\ 0 \\ 0 \end{Bmatrix} = \begin{bmatrix} 0 & 0 & A_i^c \\ A_j^a & 0 & 0 \\ 0 & A_k^b & 0 \\ 0 & -A_i^b & A_i^c \\ A_j^a & 0 & -A_j^c \\ -A_k^a & A_k^b & 0 \\ 0 & A_o^b & -A_o^c \\ A_o^a & -A_o^b & 0 \\ 0 & -A_p^b & A_p^c \\ A_q^a & 0 & -A_q^c \\ -A_r^a & A_r^b & 0 \end{bmatrix} \begin{Bmatrix} \alpha_a \\ \alpha_b \\ \alpha_c \end{Bmatrix} \qquad \text{---(4.4.3)}$$

Equation (4.4.3) is partitioned to relate the 9 local coordinates of subelement a , that is, α_a to the 9 nodal displacements, U of the complete element. Equation (4.4.4) illustrates this.

$$\begin{Bmatrix} U \\ \hline 0 \end{Bmatrix} = \left[\begin{array}{c|c} A_{11} & A_{12} \\ \hline A_{21} & A_{22} \end{array}\right] \begin{Bmatrix} \alpha_a \\ \hline \alpha_0 \end{Bmatrix} \qquad \text{---(4.4.4)}$$

where,

$$\{U\} = \begin{Bmatrix} U_i \\ U_j \\ U_k \end{Bmatrix} \quad \text{and} \quad \{\alpha_o\} = \begin{Bmatrix} \alpha_b \\ \alpha_c \end{Bmatrix}$$

From equation (4.4.4) we have

$$U = A_{11}\alpha_a + A_{12}\alpha_o \qquad \text{--- (4.4.5)}$$

$$0 = A_{21}\alpha_a + A_{22}\alpha_o \qquad \text{--- (4.4.6)}$$

Equation (4.4.6) gives the relation:

$$\alpha_o = -A_{22}^{-1} A_{21}\alpha_a \qquad \text{---(4.4.7)}$$

Substituting for α_o in equation (4.4.5), we get

$$U = A_{11}\alpha_a + A_{12}(-A_{22}^{-1} A_{21} \alpha_a)$$

$$= (A_{11} - A_{12} A_{22}^{-1} A_{21})\alpha_a$$

or,

$$U = [\bar{T}]\alpha_a \qquad \text{---(4.4.8)}$$

where,

$$[\bar{T}] = (A_{11} - A_{12} A_{22}^{-1} A_{21})$$

$$\alpha_a = [\bar{T}]^{-1} U \qquad \text{---(4.4.9)}$$

Substituting for α_o in equation (4.4.7), we get

$$\alpha_o = -A_{22}^{-1} A_{21} [\bar{T}]^{-1} U \qquad \text{---(4.4.10)}$$

Combining (4.4.9) and (4.4.10), we can write

$$\begin{Bmatrix} \alpha_a \\ \alpha_o \end{Bmatrix} = \begin{bmatrix} \bar{\bar{T}}^{-1} \\ -A_{22}^{-1} A_{21} \bar{\bar{T}}^{-1} \end{bmatrix} \{U\}$$

or,

$$\begin{Bmatrix} \alpha_a \\ \alpha_b \\ \alpha_c \end{Bmatrix} = [A]^{-1} \{U\} \qquad \text{---(4.4.11)}$$

where, U is a column vector of nodal displacements of the complete triangle, and

$$[A]^{-1} = \begin{bmatrix} \bar{\bar{T}}^{-1} \\ -A_{22}^{-1} A_{21} \bar{\bar{T}}^{-1} \end{bmatrix} \{U\}$$

The computed stiffness and mass matrices for subelement a in its local coordinate system are designated as $[k]_a$ and $[m]_a$ respectively. Similarly $[k]_b$, $[m]_b$ and $[k]_c$, $[m]_c$ represent the stiffness and mass matrices for subelements b and c in their local coordinates.

Now the local stiffness and mass matrices $[k]_L$ $[m]_L$ for every set of three subelements could be written as

$$[k]_L = \begin{bmatrix} k_a & & \\ & k_b & \\ & & k_c \end{bmatrix} \qquad \text{---(4.4.12)}$$

$$[m]_L = \begin{bmatrix} m_a & & \\ & m_b & \\ & & m_c \end{bmatrix} \quad \text{---(4.4.13)}$$

The transformation matrix $[A]^{-1}$ in equation (4.4.11) then serves to transform the stiffness and matrices of the set of three subelements in the local system to the desired nodal stiffness and mass matrices of the complete element in the datum coordinate system. That is,

$$[\bar{k}] = [A^{-1}]^T [k]_L [A^{-1}] \quad \text{----(4.4.14)}$$

$$[\bar{m}] = [A^{-1}]^T [m]_L [A^{-1}] \quad \text{----(4.4.15)}$$

$[\bar{k}]$ and $[\bar{m}]$ represent the stiffness and mass matrices respectively of the complete element in datum coordinates.

Next step is to assemble these matrices of all the triangular elements discretising the structure. The condensed stiffness and mass matrices for the entire structure are designated respectively as $[K]$ and $[M]$.

Free Vibrations:

In free vibrations, the only forces acting on the mass of an elastic system are imposed by the internal elastic forces and by D'Alembert's principle, they are equal and opposite to inertial forces (31).

External forces being absent for undamped free vibrations, an extension of equation (A.1.12) in appendix 1, namely

$$[\bar{m}]\{\ddot{U}\} + [\bar{k}]\{U\} = P$$

leads to the equation of motion for the entire structure. That is,

$$[M]\{\ddot{U}\} + [K]\{U\} = 0 \qquad \text{---(4.4.16)}$$

where,

$[M]$ = Condensed mass matrix for the entire structure,

$[K]$ = Condensed stiffness matrix for the entire structure,

$\{\ddot{U}\}$ = Nodal acceleration vector,

and $\{U\}$ = Nodal displacement vector.

Assuming for the nodal displacements a solution of the form

$$\{U\} = \{q\} \sin \omega_n t \qquad \text{---(4.4.17)}$$

where, $\{q\}$ = column vector of amplitudes of displacements $\{U\}$,

ω_n = natural frequency of free vibrations,

and t = time.

Inserting equation (4.4.17) in equation (4.4.16) we get

$$(- \omega_n^2[M]+[K])\ q = 0 \qquad \text{---(4.4.18)}$$

Premultiplying equation (4.4.18) by $[K]^{-1}$ ($1/\omega_n^2$), we get

$$((1/\omega_n{}^2)I - [K]^{-1}[M])\{q\} = 0$$

that is,

$$((1/\omega_n{}^2)I - [\bar{D}])\{q\} = 0 \qquad \text{---(4.4.19)}$$

where,

I is the identity matrix and $[\bar{D}]$ is called the Dynamical Matrix.

$$[\bar{D}] = [K]^{-1}[M] \qquad \text{---(4.4.20)}$$

Equation (4.4.19) has a non-zero solution for q provided the determinant:

$$(1/\omega_n{}^2)I - [\bar{D}] = 0 \qquad \text{---(4.4.21)}$$

The determinant in equation (4.4.21) when expanded gives a polynomial of degree n in $1/\omega_n{}^2$, where n is the number of degrees of freedom for the entire structure. The roots of this polynomial give the eigenvalues of the Dynamical Matrix $[\bar{D}]$. Reciprocals of the square root of these eigenvalues thus give n number of natural frequemcies of the system in radians per second.

Computer program is made to obtain the highest ten values of $1/\omega_n{}^2$ in this study so that first ten natural frequencies are computed(32,33).

Corresponding to each of these eigenvalues, there will be a solution of equation (4.4.19) of the form $C\, q_i$, where q_i is a non-zero vector of displacement amplitudes and C is an arbitrary constant. These solutions are the eigenvectors which represent the mode shapes.

Since the elements of an eigenvector are derived from a set of homogeneous equations, the elements can be normalised for convenience thus adjusting their sizes.In this study the eigenvectors are so normalised that the numerically largest element of each eigenvector is unity.

First ten natural frequencies and corresponding mode shapes for a square cantilever plate are presented in Table 2 and Table 3 respectively.

Table 2

FIRST TEN NATURAL FREQUENCIES OF A SQUARE CANTILEVER PLATE OF THIN UNIFORM RECTANGULAR CROSS SECTION.

NATURAL FREQUENCIES ARE EXPRESSED IN TERMS OF BETA.

3.4334E+00
8.5923E+00
2.1512E+01
2.7920E+01
3.1829E+01
5.8517E+01
6.4879E+01
6.7689E+01
7.5918E+01
1.0356E+02

Table 3

MODE SHAPE FOR BETA=3.433E+00

3.4578E-02	1.3192E-02	-8.0697E-02	1.4518E-01	1.8906E-02	-1.4929E-01
3.1505E-01	1.8503E-02	-1.9590E-01	5.2256E-01	1.5584E-02	-2.2174E-01
7.4891E-01	1.2677E-02	-2.3165E-01	9.8130E-01	1.0907E-02	-2.3289E-01
4.2334E-02	4.0344E-03	-8.3622E-02	1.5829E-01	8.5070E-03	-1.4805E-01
3.2895E-01	9.9669E-03	-1.9274E-01	5.3499E-01	9.5677E-03	-2.1871E-01
7.5951E-01	8.5774E-03	-2.2982E-01	9.9071E-01	7.5711E-03	-2.3227E-01
4.4392E-02	4.2667E-04	-8.7663E-02	1.6373E-01	2.7131E-03	-1.5064E-01
3.3598E-01	4.2804E-03	-1.9350E-01	5.4217E-01	4.8502E-03	-2.1846E-01
7.6624E-01	4.8563E-03	-2.2932E-01	9.9692E-01	4.5580E-03	-2.3182E-01
4.4592E-02	8.4678E-05	-8.8361E-02	1.6508E-01	2.3465E-04	-1.5188E-01
3.3837E-01	6.7650E-04	-1.9419E-01	5.4506E-01	1.0289E-03	-2.1872E-01
7.6928E-01	1.2708E-03	-2.2939E-01	1.0000E+00	1.3318E-03	-2.3185E-01
4.4301E-02	-5.0226E-04	-8.7850E-02	1.6427E-01	-1.7260E-03	-1.5137E-01
3.3739E-01	-2.5249E-03	-1.9417E-01	5.4424E-01	-2.5779E-03	-2.1896E-01
7.6877E-01	-2.2676E-03	-2.2970E-01	9.9981E-01	-1.9727E-03	-2.3218E-01
4.2856E-02	-2.2124E-03	-8.5256E-02	1.6048E-01	-5.8488E-03	-1.4938E-01
3.3250E-01	-7.2626E-03	-1.9383E-01	5.3951E-01	-6.8665E-03	-2.1951E-01
7.6466E-01	-5.9105E-03	-2.3039E-01	9.9633E-01	-5.2365E-03	-2.3278E-01
3.9108E-02	-6.2358E-03	-7.1563E-02	1.5124E-01	-1.3336E-02	-1.4261E-01
3.2216E-01	-1.3857E-02	-1.9195E-01	5.3040E-01	-1.1502E-02	-2.2020E-01
7.5720E-01	-8.9800E-03	-2.3159E-01	9.8995E-01	-7.7016E-03	-2.3366E-01

MODE SHAPE FOR BETA=8.5923E+00

7.1862E-02	-1.5910E-02	-1.6523E-01	2.6170E-01	-8.2786E-02	-2.2070E-01
4.8297E-01	-1.5641E-01	-2.1991E-01	6.9014E-01	-2.2139E-01	-1.8824E-01
8.6182E-01	-2.6944E-01	-1.4841E-01	1.0000E+00	-3.0036E-01	-1.2304E-01
5.0466E-02	-2.2683E-02	-1.0354E-01	1.7595E-01	-8.7486E-02	-1.4714E-01
3.2515E-01	-1.5959E-01	-1.5036E-01	4.6727E-01	-2.2546E-01	-1.3259E-01
5.8862E-01	-2.7811E-01	-1.0916E-01	6.9247E-01	-3.1835E-01	-9.8436E-02
2.4934E-02	-2.6183E-02	-5.2762E-02	8.7518E-02	-8.8940E-02	-7.4057E-02
1.6343E-01	-1.6382E-01	-7.7449E-02	2.3737E-01	-2.3454E-01	-6.9687E-02
3.0226E-01	-2.9467E-01	-5.9552E-02	3.6077E-01	-3.4702E-01	-5.7956E-02
-1.8191E-03	-2.5803E-02	-5.6283E-04	-2.2948E-03	-9.0055E-02	-4.3774E-04
-1.5656E-03	-1.6619E-01	-1.3375E-03	5.6083E-04	-2.3924E-01	-2.2697E-03
3.5899E-03	-3.0260E-01	-3.0989E-03	7.7276E-03	-3.5930E-01	-5.6010E-03
-2.8547E-02	-2.6286E-02	5.1985E-02	-9.2640E-02	-9.0317E-02	7.3514E-02
-1.6697E-01	-1.6483E-01	7.4647E-02	-2.3660E-01	-2.3551E-01	6.5377E-02
-2.9554E-01	-2.9589E-01	5.3821E-02	-3.4656E-01	-3.4791E-01	4.8696E-02
-5.6379E-02	-2.8410E-02	1.0522E-01	-1.8303E-01	-9.0253E-02	1.4490E-01
-3.2975E-01	-1.6115E-01	1.4750E-01	-4.6763E-01	-2.2734E-01	1.2886E-01
-5.8347E-01	-2.8078E-01	1.0463E-01	-6.8210E-01	-3.2131E-01	9.4957E-02
-8.5012E-02	-2.6088E-02	1.4631E-01	-2.7169E-01	-8.6605E-02	2.1333E-01
-4.8924E-01	-1.5857E-01	2.1938E-01	-6.9264E-01	-2.2414E-01	1.9143E-01
-8.6025E-01	-2.7418E-01	1.5097E-01	-9.9689E-01	-3.0865E-01	1.2849E-01

CD TOT 0055

MODE SHAPE FOR BETA=2.1512E+01

1.8249E-01	-1.2894E-02	-4.1069E-01	5.7590E-01	-1.2514E-01	-3.5810E-01
7.9356E-01	-2.2452E-01	-2.5676E-02	6.5299E-01	-2.7900E-01	3.5760E-01
1.8832E-01	-2.9312E-01	5.9757E-01	-4.3595E-01	-2.9211E-01	6.5122E-01
1.6073E-01	-2.1699E-02	-3.1558E-01	4.6332E-01	-1.0068E-01	-2.7788E-01
5.9831E-01	-1.7179E-01	1.5114E-02	4.0818E-01	-2.1690E-01	3.6497E-01
-7.5059E-02	-2.3703E-01	5.9545E-01	-7.0541E-01	-2.4382E-01	6.5803E-01
1.3968E-01	-1.6847E-02	-2.7021E-01	3.8726E-01	-5.1950E-02	-2.1613E-01
4.6737E-01	-9.1238E-02	6.2956E-02	2.3914E-01	-1.2233E-01	3.9384E-01
-2.6522E-01	-1.4345E-01	6.1025E-01	-9.0950E-01	-1.5590E-01	6.7188E-01
1.3248E-01	3.4703E-03	-2.5436E-01	3.6400E-01	5.5765E-03	-1.9782E-01
4.2467E-01	4.7037E-03	8.2318E-02	1.7823E-01	-9.7145E-04	4.1028E-01
-3.4107E-01	-9.3893E-03	6.2386E-01	-1.0000E+00	-1.3735E-02	6.8937E-01
1.4554E-01	2.3111E-02	-2.7699E-01	4.0002E-01	6.6322E-02	-2.2050E-01
4.7836E-01	1.0178E-01	6.8950E-02	2.3951E-01	1.2182E-01	4.0735E-01
-2.8080E-01	1.2808E-01	6.2848E-01	-9.4543E-01	1.3295E-01	6.9758E-01
1.7924E-01	4.4673E-02	-3.3642E-01	4.9376E-01	1.2130E-01	-2.7939E-01
6.2187E-01	1.8511E-01	2.8984E-02	4.1089E-01	2.1983E-01	3.9077E-01
-1.0097E-01	2.2968E-01	6.2699E-01	-7.6489E-01	2.3390E-01	6.9729E-01
2.3296E-01	6.0626E-02	-4.0054E-01	6.3226E-01	1.6031E-01	-3.8447E-01
8.3339E-01	2.4385E-01	-5.6004E-02	6.5929E-01	2.8036E-01	3.4810E-01
1.5545E-01	2.8283E-01	6.1811E-01	-5.0816E-01	2.8225E-01	6.9698E-01

MODE SHAPE FOR BETA=2.7920E+01

2.7875E-02	-6.4960E-02	-6.5746E-02	1.1943E-01	-1.9276E-01	-1.2884E-01
2.8813E-01	-3.2838E-01	-2.2153E-01	5.3288E-01	-4.5697E-01	-2.7202E-01
7.9066E-01	-5.5773E-01	-2.3533E-01	1.0000E+00	-6.2521E-01	-1.7531E-01
-3.3613E-02	-5.5952E-02	5.4924E-02	-6.8962E-02	-1.8226E-01	1.2002E-02
-3.5340E-02	-3.1632E-01	-8.0662E-02	8.2791E-02	-4.4155E-01	-1.5427E-01
2.3971E-01	-5.4310E-01	-1.5753E-01	3.7820E-01	-6.2048E-01	-1.2583E-01
-7.7927E-02	-3.2411E-02	1.4483E-01	-2.1443E-01	-1.0941E-01	1.2528E-01
-2.9311E-01	-1.9852E-01	3.2551E-02	-2.8166E-01	-2.8557E-01	-5.3599E-02
-2.1401E-01	-3.6158E-01	-7.9672E-02	-1.5330E-01	-4.2311E-01	-4.8476E-02
-8.8848E-02	8.1543E-03	1.7183E-01	-2.5830E-01	1.8360E-02	1.6698E-01
-3.8197E-01	1.8447E-02	8.3157E-02	-4.2074E-01	6.3669E-03	-1.0866E-03
-4.0179E-01	-1.4150E-02	-3.1699E-02	-3.9284E-01	-2.4188E-02	1.3823E-02
-5.9547E-02	4.6413E-02	1.2037E-01	-1.7584E-01	1.4188E-01	1.1421E-01
-2.5452E-01	2.3195E-01	4.6648E-02	-2.6602E-01	2.9915E-01	-1.8271E-02
-2.3688E-01	3.4012E-01	-3.3681E-02	-2.2711E-01	3.8191E-01	2.0537E-02
-6.0889E-04	6.7925E-02	1.1288E-02	-7.1168E-04	2.0465E-01	-9.1083E-03
3.4730E-02	3.4267E-01	-6.0143E-02	1.1423E-01	4.5729E-01	-9.5865E-02
2.0424E-01	5.3796E-01	-8.0053E-02	2.5862E-01	5.9825E-01	-2.4438E-02
6.7035E-02	6.2537E-02	-1.0654E-01	2.0404E-01	2.0292E-01	-1.5566E-01
3.8215E-01	3.5126E-01	-1.9458E-01	5.8231E-01	4.7892E-01	-2.0374E-01
7.5871E-01	5.7087E-01	-1.5501E-01	8.7308E-01	6.2937E-01	-8.4165E-02

CD TOT 0052

MODE SHAPE FOR BETA=3.1829E+01

2.0787E-01	-5.3541E-02	-4.6231E-01	6.0894E-01	-2.1697E-01	-2.9742E-01
7.2370E-01	-2.7825E-01	1.4351E-01	4.1439E-01	-2.0524E-01	5.3079E-01
-1.7641E-01	-5.9466E-02	6.6156E-01	-8.1759E-01	7.4620E-02	6.0078E-01
1.4345E-01	-6.5864E-02	-2.8735E-01	3.9722E-01	-2.1344E-01	-2.0401E-01
4.6100E-01	-2.6058E-01	9.2267E-02	2.3123E-01	-1.7156E-01	3.7505E-01
-2.0414E-01	7.3350E-04	4.9406E-01	-6.9792E-01	1.8131E-01	4.9103E-01
6.7352E-02	-8.1074E-02	-1.3904E-01	1.8540E-01	-2.1481E-01	-8.9997E-02
2.0876E-01	-2.5084E-01	5.9253E-02	8.0622E-02	-1.3566E-01	2.0907E-01
-1.6141E-01	8.1527E-02	2.7943E-01	-4.4834E-01	3.2779E-01	2.9634E-01
-1.2888E-02	-7.7292E-02	1.3457E-02	-2.3994E-02	-2.0775E-01	1.3023E-02
-2.8587E-02	-2.3066E-01	9.6435E-03	-3.2507E-02	-9.6186E-02	1.1851E-02
-4.4797E-02	1.4834E-01	1.9797E-02	-7.2184E-02	4.2830E-01	3.8939E-02
-8.7148E-02	-7.0381E-02	1.5645E-01	-2.1915E-01	-1.8749E-01	1.0689E-01
-2.4220E-01	-2.0269E-01	-4.8980E-02	-1.1432E-01	-7.1422E-02	-1.9286E-01
1.1033E-01	1.6047E-01	-2.4887E-01	3.5491E-01	4.2185E-01	-2.3765E-01
-1.5659E-01	-6.9169E-02	2.8604E-01	-3.9694E-01	-1.7330E-01	1.8824E-01
-4.3487E-01	-1.8840E-01	-1.0443E-01	-1.8689E-01	-7.6000E-02	-3.7742E-01
2.4815E-01	1.1689E-01	-4.8389E-01	7.2801E-01	3.1566E-01	-4.7885E-01
-2.2850E-01	-7.4056E-02	3.8738E-01	-5.6837E-01	-1.7996E-01	2.9162E-01
-6.2585E-01	-2.0485E-01	-1.1648E-01	-2.7494E-01	-1.0458E-01	-5.1691E-01
3.3807E-01	6.5841E-02	-6.7710E-01	1.0000E+00	2.2636E-01	-6.5626E-01

MODE SHAPE FOR BETA=5.8517E+01

2.9176E-01	-2.0457E-01	-6.3395E-01	7.7455E-01	-5.4246E-01	-2.3318E-01
7.4158E-01	-5.0874E-01	4.2332E-01	1.7608E-01	-1.1306E-01	7.5916E-01
-5.1887E-01	3.8185E-01	5.9278E-01	-1.0000E+00	7.4955E-01	3.2047E-01
8.1980E-02	-2.0504E-01	-1.8949E-01	2.3533E-01	-5.5466E-01	-9.1015E-02
2.2639E-01	-5.4682E-01	1.3545E-01	5.0818E-02	-1.5038E-01	2.2753E-01
-1.2976E-01	3.9789E-01	1.2880E-01	-2.1117E-01	8.5423E-01	4.1238E-02
-9.8664E-02	-1.5010E-01	1.6558E-01	-2.3472E-01	-3.9167E-01	1.0867E-01
-2.6004E-01	-4.2878E-01	-4.6448E-02	-1.1411E-01	-1.7738E-01	-2.4150E-01
1.8269E-01	2.3128E-01	-3.5691E-01	5.3647E-01	6.1402E-01	-3.5079E-01
-1.6058E-01	2.2691E-02	3.0341E-01	-4.2341E-01	1.1228E-02	2.1796E-01
-4.9908E-01	-4.4282E-02	-7.5092E-02	-2.5162E-01	-8.3958E-02	-4.2874E-01
2.6108E-01	-5.7699E-02	-6.0412E-01	8.6265E-01	-4.2360E-03	-6.1436E-01
-5.0273E-02	1.9075E-01	1.1866E-01	-1.9745E-01	4.3779E-01	1.6869E-01
-3.2344E-01	4.0161E-01	5.9203E-02	-2.5001E-01	1.0131E-01	-2.2556E-01
9.2188E-02	-2.6091E-01	-4.6273E-01	5.9199E-01	-5.5811E-01	-5.5217E-01
1.8292E-01	2.7255E-01	-2.9678E-01	3.3764E-01	6.3481E-01	-1.6218E-02
1.8962E-01	6.2931E-01	2.7587E-01	-8.3141E-02	2.3719E-01	2.3692E-01
-1.8277E-01	-2.8306E-01	-4.0487E-02	-4.4339E-02	-7.0443E-01	-2.2558E-01
4.4478E-01	2.5018E-01	-7.2348E-01	9.4514E-01	6.0374E-01	-3.1312E-01
8.0903E-01	6.2577E-01	4.4304E-01	1.6804E-01	2.6400E-01	7.5062E-01
-4.3711E-01	-2.3560E-01	4.8214E-01	-7.1917E-01	-6.4183E-01	1.5303E-01

CD TOT 0052

MODE SHAPE FOR BETA=6.4879E+01

1.7338E-01	5.8042E-02	-3.6513E-01	2.9676E-01	4.4760E-02	2.0899E-01
-6.7631E-02	6.5890E-02	5.3898E-01	-3.7219E-01	6.3587E-02	-3.5904E-02
-1.5750E-02	-1.9454E-02	-7.6798E-01	8.0815E-01	-1.3892E-01	-8.7129E-01
2.1572E-01	3.7542E-02	-3.9060E-01	3.5324E-01	6.0173E-02	1.3289E-01
4.3135E-03	7.2270E-02	5.3698E-01	-3.3545E-01	2.0785E-02	1.0860E-01
-8.9664E-02	-1.1183E-01	-5.9468E-01	6.1066E-01	-2.6407E-01	-7.8989E-01
2.4278E-01	2.3556E-02	-4.3939E-01	4.1591E-01	6.2165E-02	1.0729E-01
7.2599E-02	5.9970E-02	5.5919E-01	-3.2337E-01	4.8206E-03	2.0702E-01
-1.9187E-01	-8.7150E-02	-4.6489E-01	3.8315E-01	-1.8183E-01	-6.6997E-01
2.5277E-01	2.7675E-03	-4.6248E-01	4.4947E-01	4.5925E-03	8.5460E-02
1.1242E-01	1.1810E-02	5.6947E-01	-3.0625E-01	2.3687E-02	2.4799E-01
-2.1548E-01	3.9511E-02	-4.1763E-01	3.1346E-01	5.9916E-02	-6.1605E-01
2.4074E-01	-1.8816E-02	-4.4408E-01	4.2263E-01	-5.7668E-02	9.3560E-02
8.9571E-02	-6.5480E-02	5.5290E-01	-2.9373E-01	-6.4878E-03	1.9666E-01
-1.4109E-01	1.0573E-01	-4.8817E-01	4.5739E-01	2.3309E-01	-6.8039E-01
2.2666E-01	-1.4089E-04	-4.0976E-01	3.6453E-01	-5.5530E-02	1.4725E-01
-1.8816E-03	-1.2283E-01	5.6038E-01	-3.4593E-01	-1.0429E-01	1.0495E-01
-7.2958E-02	3.0786E-02	-6.3655E-01	6.7468E-01	1.9024E-01	-8.3613E-01
2.3778E-01	3.5544E-02	-4.0077E-01	3.1627E-01	-3.4013E-02	1.7655E-01
-1.3356E-01	-1.5322E-01	6.3748E-01	-4.8470E-01	-1.8789E-01	1.1659E-01
-1.0004E-01	-8.2897E-02	-7.5557E-01	7.9834E-01	4.5692E-02	-1.0000E+00

MODE SHAPE FOR BETA=6.7689E+01

2.1058E-02	1.1359E-01	-3.3673E-02	-6.2105E-02	3.1077E-01	2.5300E-01
-3.8806E-01	5.6870E-01	4.1809E-01	-7.0488E-01	7.9653E-01	1.7151E-01
-7.0116E-01	8.9193E-01	-2.3251E-01	-3.9918E-01	8.8071E-01	-3.6155E-01
1.0597E-01	5.7174E-02	-1.8740E-01	2.0026E-01	2.0432E-01	7.7868E-03
1.0898E-01	4.1718E-01	1.6937E-01	-5.2392E-03	6.0252E-01	4.5418E-02
7.6203E-02	6.6376E-01	-2.1149E-01	3.6023E-01	6.0926E-01	-3.3224E-01
9.9913E-02	-6.3570E-02	-1.9226E-01	2.4035E-01	-1.2091E-01	-8.8398E-02
2.6880E-01	-9.3957E-02	2.0215E-02	2.6228E-01	-6.1525E-02	-3.1256E-02
3.4819E-01	-1.1454E-01	-1.6287E-01	5.6079E-01	-2.8094E-01	-2.7411E-01
3.1541E-03	-1.2450E-01	-1.9598E-02	1.9329E-02	-3.1254E-01	-9.4708E-03
1.3212E-02	-4.0281E-01	1.6470E-02	-1.0324E-02	-4.6215E-01	8.7264E-03
-1.6105E-02	-5.9012E-01	-2.7778E-02	2.2071E-02	-8.1382E-01	-9.1171E-02
-8.4752E-02	-5.3476E-02	1.5163E-01	-1.9789E-01	-1.2461E-01	8.6252E-02
-2.4443E-01	-1.0762E-01	2.2210E-02	-2.8025E-01	-6.4117E-02	5.2088E-02
-3.7376E-01	-1.0828E-01	1.2329E-01	-5.3716E-01	-2.3506E-01	1.8080E-01
-8.3643E-02	4.7875E-02	1.5874E-01	-1.6931E-01	1.6724E-01	2.1634E-02
-1.0861E-01	3.6772E-01	-1.1851E-01	-1.8189E-02	5.8072E-01	-4.2385E-02
-7.8952E-02	6.9116E-01	1.7101E-01	-3.3777E-01	7.0037E-01	3.5309E-01
-2.5016E-02	5.9576E-02	5.0733E-02	4.1161E-02	2.3991E-01	-1.5045E-01
3.2752E-01	4.9583E-01	-3.7117E-01	6.5441E-01	7.6096E-01	-2.7473E-01
7.3711E-01	9.3430E-01	7.0037E-02	5.0998E-01	1.0000E+00	3.5187E-01

CD TOT 0054

MODE SHAPE FOR BETA=7.5918E+01

3.4171E-01	-1.1630E-01	-7.1544E-01	6.8899E-01	-3.5011E-01	1.9101E-01
2.4167E-01	-2.7677E-01	7.6244E-01	-2.5846E-01	-1.2603E-01	1.0028E-01
1.3405E-02	-1.4569E-01	-7.6901E-01	8.2669E-01	-2.8692E-01	-8.4889E-01
2.0787E-01	-1.3998E-01	-3.9971E-01	3.5442E-01	-3.4424E-01	1.5226E-01
-1.1301E-02	-2.4083E-01	5.6926E-01	-3.7450E-01	-8.3703E-02	1.1307E-01
-1.4921E-01	-1.5038E-01	-5.7771E-01	5.0086E-01	-3.6855E-01	-7.1902E-01
7.6286E-02	-1.1933E-01	-1.4828E-01	9.4384E-02	-1.9375E-01	1.4440E-01
-1.3310E-01	-7.5428E-03	3.2318E-01	-3.2903E-01	1.8845E-01	4.1228E-02
-1.7954E-01	1.0466E-01	-3.6182E-01	2.2120E-01	-1.7022E-01	-4.3860E-01
-1.7655E-02	-7.3034E-02	2.2507E-02	-2.8690E-02	-6.9054E-02	2.6654E-02
-3.9476E-02	1.8697E-01	1.4868E-02	-3.9343E-02	3.9770E-01	-3.0313E-02
6.2508E-03	2.7278E-01	-8.3821E-02	9.7446E-02	-7.0357E-02	-9.4974E-02
-9.5531E-02	-8.7015E-02	1.6126E-01	-1.1311E-01	-1.1173E-01	-1.1239E-01
1.0052E-01	9.2735E-02	-2.9080E-01	2.7596E-01	2.4189E-01	-7.1896E-02
1.7754E-01	7.3191E-02	2.3614E-01	-8.3251E-02	-3.1123E-01	2.7391E-01
-2.0746E-01	-1.4243E-01	3.4976E-01	-2.8799E-01	-2.4376E-01	-1.8683E-01
8.2347E-02	-1.2015E-01	-5.2010E-01	3.7596E-01	-2.4404E-02	-6.4306E-02
1.1046E-01	-2.0099E-01	5.5390E-01	-5.0235E-01	-5.3784E-01	6.4660E-01
-3.4888E-01	-1.5083E-01	5.6769E-01	-5.3230E-01	-2.5818E-01	-1.1852E-01
-6.8877E-02	-1.6589E-01	-6.9017E-01	3.1168E-01	-7.6444E-02	-1.3185E-01
-9.5422E-02	-2.0300E-01	7.8481E-01	-1.0000E+00	-4.4706E-01	9.7742E-01

MODE SHAPE FOR BETA=1.0356E+02

2.9984E-03	1.7287E-01	2.1939E-02	-1.7012E-01	4.5342E-01	3.8814E-01
-5.0278E-01	6.0858E-01	2.1202E-01	-4.1257E-01	3.0139E-01	-5.3990E-01
2.6757E-01	-3.5723E-01	-8.4755E-01	1.0000E+00	-9.2467E-01	-5.5841E-01
1.1493E-01	4.6935E-02	-1.9774E-01	1.9713E-01	2.6414E-01	5.4762E-02
5.8663E-02	5.1911E-01	2.1503E-01	-9.6453E-02	3.5484E-01	6.4477E-02
-7.0682E-02	-3.0550E-01	-1.1945E-01	5.6162E-02	-9.8007E-01	-1.3921E-01
3.9171E-02	-1.9366E-01	-1.0006E-01	1.8246E-01	-2.9860E-01	-1.7753E-01
3.0189E-01	-4.2439E-02	-4.5543E-02	1.8869E-01	2.0467E-01	2.7051E-01
-1.6568E-01	1.0031E-01	4.3430E-01	-5.6633E-01	-1.9726E-01	3.8691E-01
-1.6831E-01	-2.1314E-01	2.7039E-01	-2.2978E-01	-5.0884E-01	-1.5717E-01
3.9432E-02	-4.6968E-01	-3.7333E-01	2.4469E-01	-1.0034E-01	-3.1053E-02
5.7961E-02	3.1588E-01	3.9921E-01	-3.8625E-01	5.8299E-01	5.2086E-01
-2.1804E-01	1.1100E-01	4.0145E-01	-4.4456E-01	9.3057E-02	3.0258E-02
-2.7767E-01	-1.3766E-01	-3.7132E-01	7.3084E-02	-2.2718E-01	-3.2375E-01
2.2500E-01	1.0857E-02	1.6665E-02	1.2276E-01	3.8197E-01	1.8965E-01
4.6672E-02	4.1138E-01	-2.4101E-02	-1.4516E-02	7.6449E-01	1.1628E-01
-1.1671E-01	4.6791E-01	5.5093E-02	-9.2200E-02	-8.9447E-02	-1.0165E-01
4.2660E-02	-3.6026E-01	-1.5095E-01	1.9563E-01	-2.8375E-01	-1.6505E-01
4.3339E-01	3.6091E-01	-6.6835E-01	7.5730E-01	7.9987E-01	-6.0765E-02
4.3014E-01	6.2570E-01	5.6677E-01	-1.0981E-01	3.9802E-02	4.9696E-01
-3.4195E-01	-4.1441E-01	5.1752E-02	-2.1109E-01	-5.2968E-01	-2.5318E-01

CD TOT 0052

Table 4

Comparison of Natural Frequencies of A Square Cantilever Plate of Uniform Rectangular Cross-Section.

Mode No.	Values of $\beta = \omega_n \sqrt{Dg/\rho t^4}$						
	Dana Young Energy	Zienkie-wicz** 5x5	Present Study** 5x5	Present Study** 6x6	Rawtani** 5x5	Rawtani** 6x6	Dawe* 3x3
1	3.494	3.469	3.436	3.433	3.445	3.451	3.470
2	8.547	8.535	8.640	8.592	8.516	8.502	8.530
3	21.440	21.450	21.779	21.512	21.181	21.161	21.670
4	27.460	27.059	28.147	27.920	26.919	26.968	26.850
5	31.170	------	32.216	31.829	31.052	31.029	30.800

** Structural idealization by triangular elements.

* Structural idealization by rectangular elements.

Table 5

Comparison of Natural Frequencies and Nodal Lines of Canti-levered Rectangular Plates.

Nodal Lines \ a/b	1/2	1	2	5	Results of
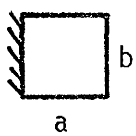	3.508	3.494	3.472	3.450	B
	3.496	3.433	3.353	3.184	P
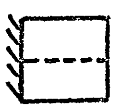	5.372	8.547	14.930	34.730	B
	5.407	8.592	15.102	35.344	P
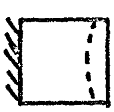	21.960	21.440	21.610	21.520	B
	23.138	21.512	21.133	20.078	P
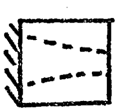	10.260	27.460	94.490	563.900	B
	10.520	27.920	96.220	----	P
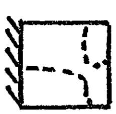	24.850	31.170	48.710	105.900	B
	25.954	31.828	49.974	110.627	P

B = Results of Barton.

P = Results of Present Investigation.

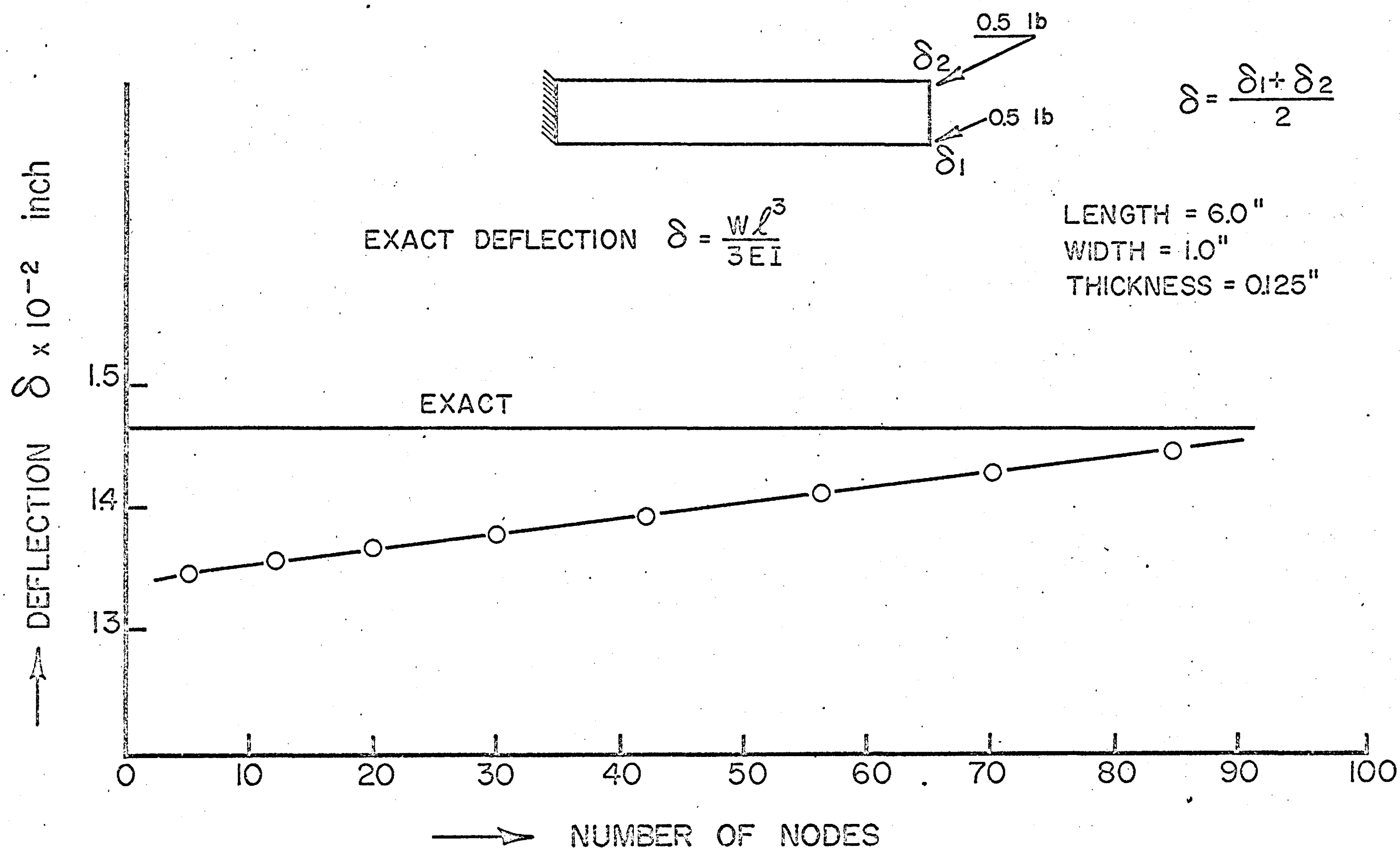

FIG. 9 MONOTONIC CONVERGENCE OF THE DISPLACEMENT PATTERN USED IN THIS INVESTIGATION PROVING THE VALIDITY OF THE STIFFNESS MATRIX OBTAINED.

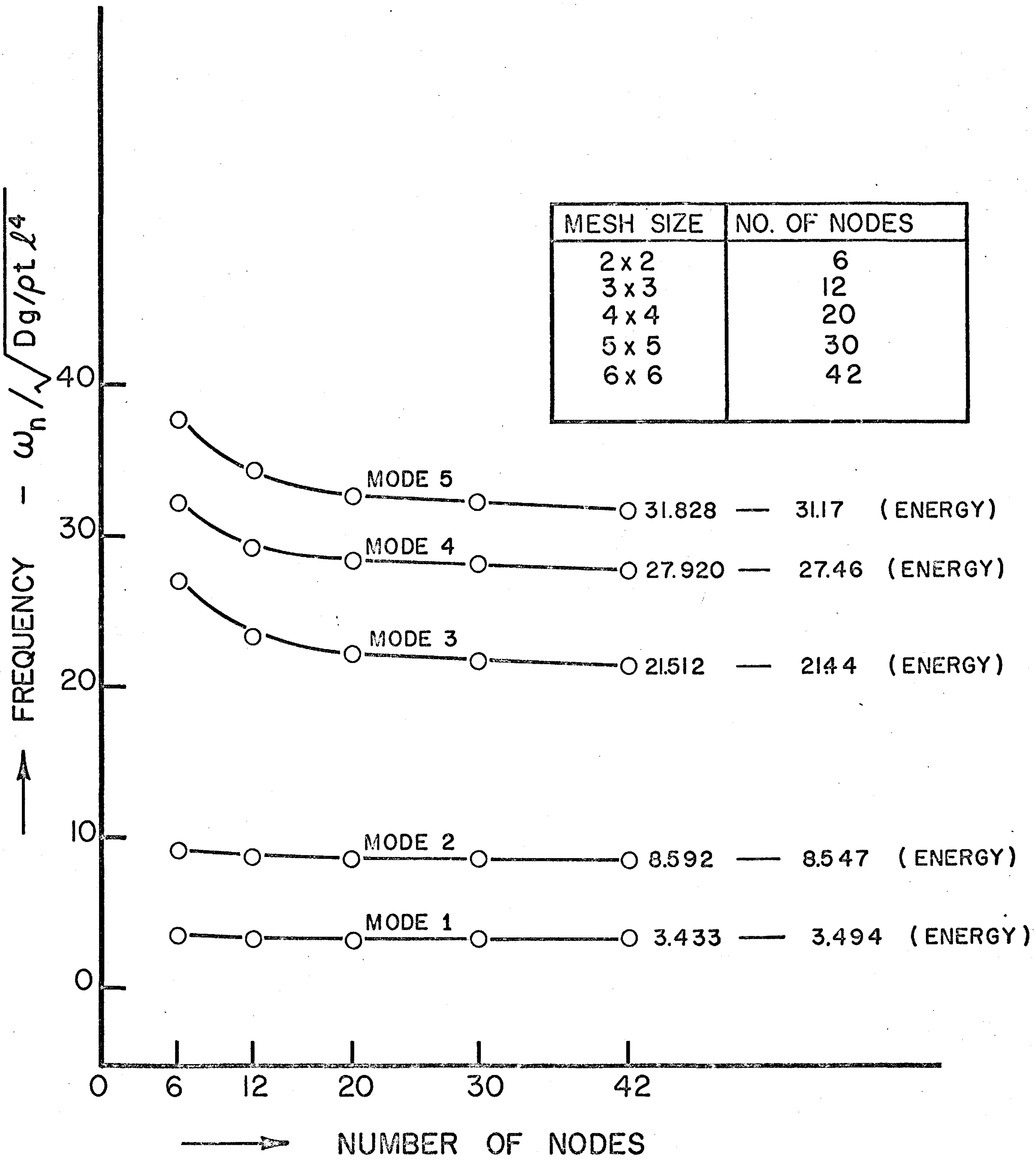

FIG. 10 EIGENVALUE CONVERGENCE FOR A SQUARE CANTILEVER PLATE

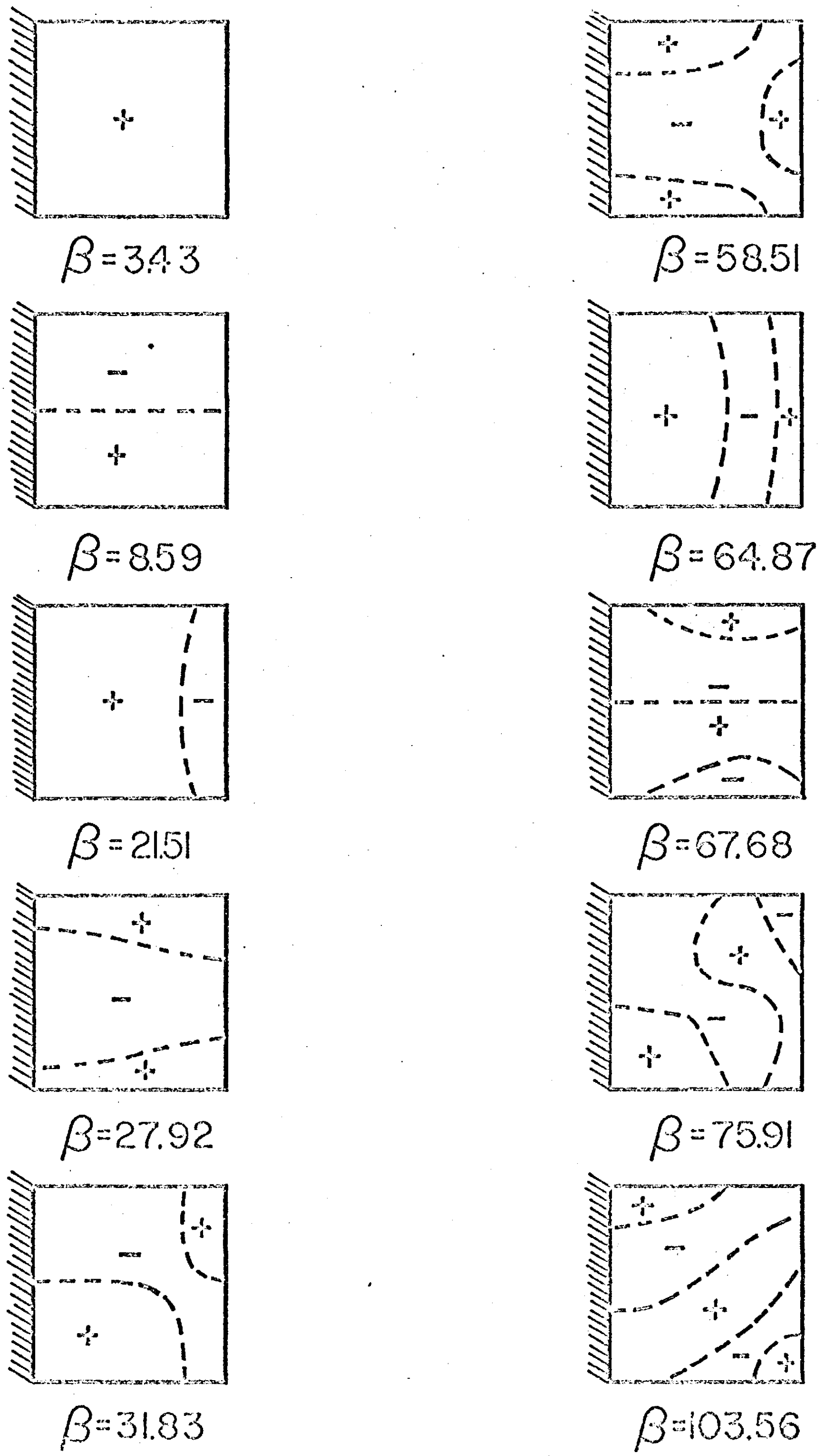

FIG. 11 ANALYTICAL NODAL PATTERNS FOR A SQUARE CANTILEVER PLATE OF UNIFORM THIN RECTANGULAR CROSS SECTION.

NATURAL FREQUENCY, $\omega_n = \frac{\beta}{\ell^2}\sqrt{\frac{Dg}{\rho t}}$

5. RESULTS AND CONCLUSIONS

The experimentally determined first natural frequency for a 6"x2"x1/16" thick mild steel cantilever without pretwist is 54.5 cycles per second. This compares reasonably well with the theoritically obtained value of 58.4 cycles per second. The plate formula (28) for an aspect ratio of three has been used to find this theoritical value.

It is difficult to achieve the ideal conditions for the fixed end of the cantilever. This ultimately makes the cantilever less rigid. Hence the experimental value is less than the calculated one.For the same boundary conditions, the same plate but with a total pretwist at the tip of 20 degrees, the cantilever becomes stiffer due to the increase in its torsional stiffness. This explains why the experimental first natural frequency of the twisted cantilever is 59.5 cycles per second which is well above that for the one without pretwist.

Table 2 and Table 3 show the computed values of first ten natural frequencies in ascending order and the corresponding mode shapes respectively, for a square cantilever plate of thin uniform rectangular cross section. Computations were made by idealising the square plate into a 6x6 mesh by triangular elements. Three degrees of freedom at each node resulted in a total of 126 algebraic simultaneous, homogeneous equations, while determining the elastic and inertial properties of the entire cantilever.

Figure 10 shows reasonable convergence of the eigenvalues at 6x6 mesh size. But no attempt was made to carry out the computations for a finer mesh. This is because of the limitation posed by the storage capacity of the computer. Computations were carried out on a CDC 6400 digital computer.

The results thus obtained are compared with results obtained by other researchers in Table 4. They are found to be in good agreement with a maximum of 2.1 percent error from Dana Young's energy solution (28). But for the first natural frequency, all frequencies are slightly higher than the energy results. This discrepancy cannot be reasoned out very easily. Furthermore, no researcher has yet solved the dynamic problem with fully compatible triangles and hence cannot be checked. Dawe's results (34) with rectangular elements also indicate a similar question that why the third natural frequency (second flexural) is higher than the energy solution? It is suspected that Zienkiewicz (35) might have had similar doubts resulting in not publishing the fifth natural frequency (second torsion).

Table 5 shows a comparison of natural frequencies and nodal lines of rectangular cantilever plates. The nodal patterns shown in Figure 11 are in good agreement with other's results.

It is seen that the phisical dimensions of cantilevers chosen for experiments and theoritical investigation are quite different. Since beam formula has been used to compare the theoritical static deflection of the cantilever, a cantilever of a large aspect ratio has been chosen. The experimental model was chosen to be quite thin in order that not too high sinusoidal exciting force was expected from the shaker used. The Eigenvalue problem was solved for a square cantulever plate so that the results of the present analysis could be easily compared with similar results obtained by other investigators.

It is concluded that the structural idealisation through fully compatible triangles has the advantage of monotonic convergence as shown in figure 9. This triangular element provides with satisfactory results when used in finite element analysis of plate vibration. Further improvement seems possible by employing additional nodal points in defining the degrees of freedom of the structure.

6. REFERENCES

1. Dokainish,M.A. and Jagannath,D.V.,"Experimental Investigation of Gas Turbine Blade Vibration-A Review", Paper to be presented at the ASME Vibration Conference, March 31-April 2, 1969.

2. Carnegie,W.,"Dynamically Isolated Vibration Test Rig", Engineering,Vol.187. Jan. 1959. pp.54-55.

3. Belgaumkar,B.M. and Lakshminarayana,K.,"Vibration Characteristics of Axial Flow Compressor Blades", J.Soc.Engg.Res., Vol.VI,Part 2, 1962, pp. 153-168.

4. Vuksta,Jr.,T.,"Experimental Techniques and Fixture Design Related to steam Turbine Blade Frequency Measurements", Experimental Mechanics,Vol.3, July 1963, pp.161-167.

5. Armstrong,E.K., "Recent Blade Vibration Techniques", ASME Meeting, Nov.27-Dec.1,1966, Paper No.66-WA/GT-14.

6. Nutt,D.A.,"Experimental Investigation of the Natural Modes of Vibration of Gas Turbine Blades",Engineering, Vol.170, 1950, p.323.

7. French,R.F.,"Mechanical Evaluation Of Gas Turbine Blades in Their Actual Centrifugal Field",Experimental Mechanics, Vol.2, April 1962, pp.122-128.

8. Truman,J.C.,Martin,J.R.and Klint,R.V.,"Pulsed-Air Vibration Technique for Testing High Performance Turbomachinery Blading",Experimantal Mechanics,Vol.1,June 1961,pp.201-205.

9. Eccles,E.S. and Seymour,D.G.,"Measuring Gas Turbine Blade Vibration", Engineering, Vol.193,March 2, 1962,pp.318-319.

10. Bose,B.N.,"Methods of Simulating Vibration of Magnetic or Non-Magnetic Blades in the Laboratory", Instrument Soc. of America, Preprint No. 133-LA-61, 1961.

11. Voysey,R.G.,"Some Blade Vibration Problems in Gas Turbine Engines", Proc. Instn. Mech. Engrs.,Vol.153,1945, pp.483-495.

12. Fangman,C.N.,Zastrow,V.A.and Bobeck,J.E.,"High Speed Turbocharger Blade Vibration Measurement",ASME Meeting, Nov.29-Dec.4,1964, Paper No.64-WA/OGP-1.

13. Starer,R.L.,"Electro Optical Tracking Techniques", Instruments and Control Systems,Reprinted from Feb.1967 issue.

14. Armstrong,E.K. and Stevenson,R.E.,"Some Practical Aspects of Compressor Blade Vibration",J.Royal Aero.Soc.,Vol.64, No.591, March 1960, pp.117-130.

15. Danforth,C.E. and Anderson,B.R., "Vibrating Stress Measurements in Multistage Compressor Blading", Proc. Soc. Exp. Stress Anal.,Vol.XIV,No.1,1955,pp.21-34.

16. Morley,D.A.,"Vibration Measurements in Gas Turbine Blades", Instruments and Control Systems, Vol.33,Feb.1960,pp.254-257.

17. Drew,D.A.,"The Measurement of Turbine Stresses in Aircraft Engines, in the Laboratory, on the Test Bed and in Flight", Proc. Soc. Exp. Stress Anal., Vol.X,No.1,1952, pp.187-202.

18. Rissone,R.F. and Burrough,H.L.,"Measurement of Blade Vibration in a Steam Turbine Under Load",The Engineer, Vol.217, January 31, 1964, pp.209-215.

19. Drew,D.A.,"Developments in Methods of Measuring Stresses in Compressor and Turbine Blades on Test Bed And in Flight", Proc.Instn.Mech.Engrs.,Vol.172,No.8,1958,pp.320-359.

20. Grinsted,B.,"Nodal Pattern Analysis", Proc.Instn.Mech.Engrs., Vol.166,1952,pp.309-321.

21. Pearson,H.,"The Aerodynamics of Compressor Blade Vibration", Fourth Anglo-American Aeronautical Conference,1953,pp.127-162.

22. Blackwell,B.D.,"Some Investigations in The Field of Blade Engineering", J.Royal Aero.Soc.,Vol.62,No.573,Sept.1958, pp.633-646.

23. Hanson,M.P.,Meyer,A.J. and Manson,S.S.,"A method of Evaluating Loose Blade Mounting as a means of Suppressing Turbine and Compressor Blade Vibration",Proc.Soc.Exp.Stress Anal., Vol.X,No.2,Nov.1950,pp.103-116.

24. Hanson,M.P.,"A Vibrating Damper for Axial Flow Compressor Blading", Proc.Soc.Exp.Stress Anal.,Vol.XIV,No.1,Nov.1955,pp.155-162.

25. DiTaranto,R.A.," A Blade Vibration Damping Device: Its Testing and a Preliminary Theory of its Operation", Journal of Applied Mech., Vol.25,1958, pp.21-27.

26. Carnegie,W.," Static Bending of Pretwisted Cantilever Blading", Proc. Instn. Mech. Engrs., Vol.171,No.32,1957,pp.873-894.

27. Carnegie,W.," Vibrations of Pretwisted Cantilever Blading", Proc. Instn. Mech. Engrs., Vol.173,No.12,1959, pp.343-374.

28. Harris,C.M. and Crede,C.E., "Shock and Vibration Handbook", Vol.1, McGraw Hill, 1961.

29. Przemieniecki,J.S., " Theory of Matrix Structural Analysis", McGraw Hill, 1968.

30. Clough,R.W. and Tocher, J.L., "Finite Element Stiffness Matrices for Analysis of Plate Bending", AFFDL-TR-66-80,pp.515-545.

31. Hurty,W.C. and Rubinstein,M.F.,"Dynamics of Structures", Prentice Hall, 1964.

32. Tiwari, M.Engg. Thesis Submitted to McMaster University,Hamilton, Ontario, 1968.

33. Froberg,C.E.,"Introduction to Numerical Analysis", Addison Wesley, 1965.

34. Dawe,D.J., "A Finite Element Approach to Plate Vibration Problems", J. of Mech. Engg. Sc., Vol.7,No.1,pp.28-32.

35. Zienkiewicz,O.C. and Cheung,Y.K., "The Finite Element Method in Structural and Continnuum Mechanics", McGraw Hill,1967.

7. APPENDICES

APPENDIX 1: Derivation of Elastic and Inertial Properties of a Triangular Element in Bending.

DERIVATION OF ELASTIC AND INERTIAL PROPERTIES OF A TRIANGULAR ELEMENT IN BENDING.

The elastic and inertial properties of the idealised structural element have been determined in this study by using the principle of virtual work for dynamic conditions.

The structural element considered is a triangular plate element as shown in Figure 8. It is assumed that the element properties are specified for three z-deflections, three x-rotations and three y-rotations. For convenience both deflections and rotations will be referred to as displacements.

The first assumption made is that the interior displacements, $u = \{u_x \;\; u_y \;\; u_z\}$ can be expressed in terms of the discrete displacements $U = \{U_1 \;\; U_2 \; \ldots \; U_9\}$ by the approximate matrix equation:

$$u = \bar{a}U \qquad \text{--(A.1.1)}$$

where, $\bar{a} = \bar{a}(x,y,z)$, a function of local coordinates.

The total strains e, obtained by differentiation of equation (A.1.1) leads to matrix equation:

$$e = \bar{b}U \qquad \text{--(A.1.2)}$$

At any particular instant of time, we can assume that the displacements u acquire virtual displacements δu, which are infinetesimal and arbitrary, but compatible with the boundary conditions on the body. Virtual displacements produce virtual

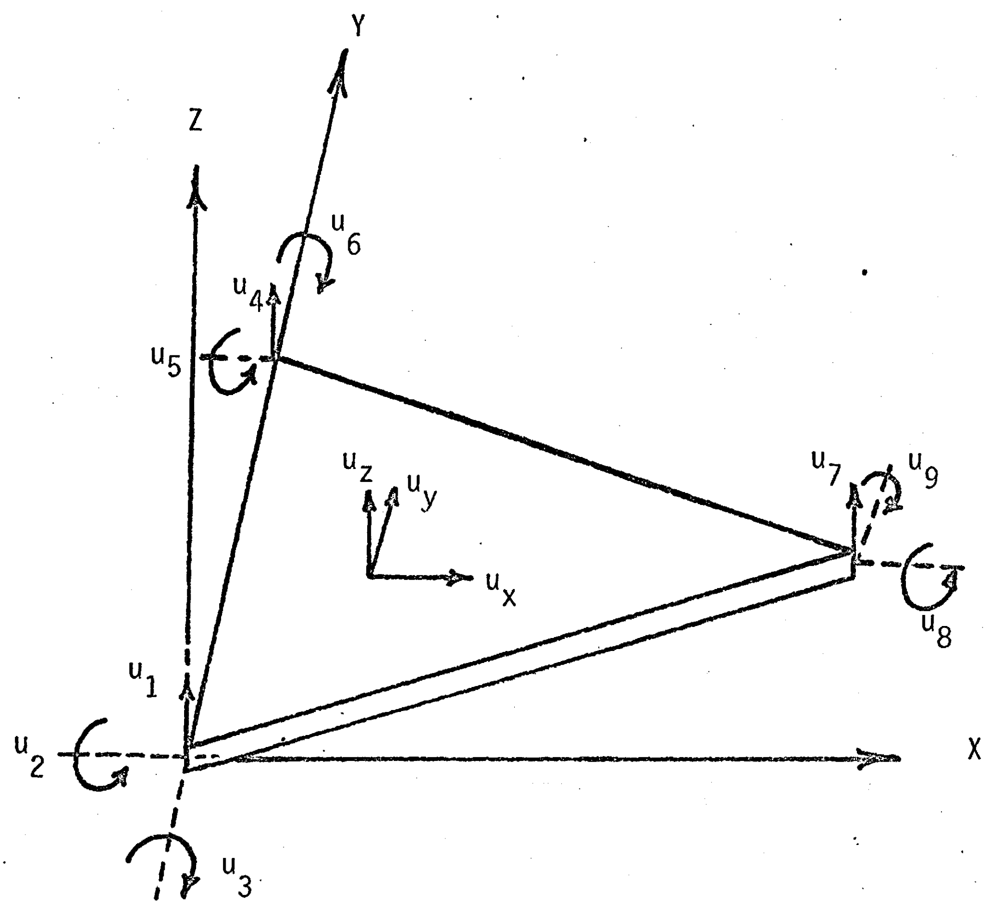

FIG. 8. TRIANGULAR ELEMENT IN BENDING SHOWING NINE DEGREES OF FREEDOM.

strains $\delta\varepsilon$ from which, the virtual strain energy δU_i can be calculated for a known stress distribution. Virtual work in case of a dynamic system includes the work done by inertia forces along with the virtual work of external forces, if any.

By principle of virtual work:

Virtual strain energy = Virtual work + work done by inertia forces

That is, $$\delta U_i = \delta W - \int_V \rho \delta u^T \ddot{u} \, dv \qquad \text{--- (A.1.3)}$$

Total strain = Elastic strain + Thermal strain + Initial strain

That is, $e = \varepsilon + e_T + e_I$

$$\delta e = \delta\varepsilon + \delta e_T + \delta e_I$$

Assuming $\delta e_T = \delta e_I = 0$, We get $\delta e = \delta\varepsilon$ --- (A.1.4)

Virtual displacements and virtual strains which could be obtained from equations (A.1.1) and (A.1.2) are respectively

$$\delta u = \bar{a} \; \delta U \qquad \text{--- (A.1.5)}$$

and $$\delta e = \bar{b} \; \delta U$$

Sustituting for δe from equation (A.1.4)

$$\delta\varepsilon = \bar{b} \; \delta U \qquad \text{--- (A.1.6)}$$

By definition, Virtual strain energy:

$$\delta U_i = \int_V \delta\varepsilon^T \sigma \, dv \qquad \text{--- (A.1.7)}$$

By definition of Hooke's law

$$\text{Stress } \sigma = Xe + \bar{\alpha} T X_T \qquad \text{--- (A.1.8)}$$

for a specified temperature distribution $T=T(x,y,z)$,

where, X represents the material stress strain relationships

$$X = \frac{E}{1-\nu^2}\begin{bmatrix} 1 & \nu & 0 \\ \nu & 1 & 0 \\ 0 & 0 & \frac{1-\nu}{2} \end{bmatrix} ,$$

E and ν being the Young's modulus and Poisson's ratio. Also, $\bar{\alpha}TX_T$ represents stress necessary to suppress thermal expansion.

Substituting for e from (A.1.2) in (A.1.8) and substituting for σ in (A.1.7), we get the virtual strain energy:

$$\delta U_i = \int_V \delta U^T \bar{b}^T X \bar{b}U \, dv + \int_V \delta U^T \bar{b}^T X_T \alpha T \, dv \quad \text{--- (A.1.9)}$$

Virtual work = $\delta W = \delta U^T P$ --- (A.1.10)

where, P is the external force vector

from equation (A.1.1),

work done by inertia forces = $-\int \rho \delta U^T \bar{a}^T \bar{a} \ddot{U} \, dv$ ---(A.1.11)

Inserting equations (A.1.9), (A.1.10) and (A.1.11) in equation (A.1.3) gives:

$$\int_V \delta U^T \bar{b}^T X\bar{b}U \, dv + \int_V \delta U^T \bar{b}^T X_T \alpha T \, dv = \delta U^T P - \int_V \rho \delta U^T \bar{a}^T \bar{a} \ddot{U} \, dv$$

that is, $[M]\{\ddot{U}\} + [K]\{U\} = P$ ---(A.1.12)

where, $[M] = \int_V \rho \bar{a}^T \bar{a} \, dv$ --- (A.1.13)

= mass matrix of the equivalent discrete system.

$[K] = \int_V \bar{b}^T X \bar{b} \, dv$ --- (A.1.14)

= stiffness matrix of the equivalent discrete system.

The element displace ments in the normal direction are expressed in terms of assumed displacement patterns. In the present investigation, it is:

$$u_z = \alpha_1 + \alpha_2 x + \alpha_3 y + \alpha_4 x^2 + \alpha_5 xy + \alpha_6 y^2 + \alpha_7 x^3 + \alpha_8 xy^2 + \alpha_9 v^3 \quad \text{--(A.1.15)}$$

for subtriangle a.

Equation (A.1.15) can be written in the matrix form:

$$\{u_z\} = \begin{bmatrix} 1 & x & y & x^2 & xy & y^2 & x^3 & xy^2 & y^3 \end{bmatrix} \begin{Bmatrix} \alpha 1 \\ \alpha_2 \\ \vdots \\ \alpha_9 \end{Bmatrix}$$

or $u = \bar{c}\alpha$ where $\bar{c} = \bar{c}(x,y,z)$

element strains e are computed and put in the matrix form

$$e = \bar{d}\alpha$$

where $\bar{d}$ is obtained by appropriate differentiation of c.

The element bending stiffness k in its local coordinates can now be computed by using (A.1.14)

$$[k] = \int_V \bar{d}^T X \bar{d} \, dv$$

In matrix form the displacement u_z normal to the middle plane of the element in datum coodinates is written

$$u_z = a_z U \quad \text{--- (A.1.16)}$$

The displacements u_x and u_y caused by rotations of normal to the middle plane are calculated by differentiating the expression for u_z w.r.t x and y and can be put in matrix form

$$u_x = a_x U \quad \text{--- (A.1.17)}$$

$$u_y = a_y U \quad \text{--- (A.1.18)}$$

Equations (A.1.16), (A.1.17) and (A.1.18) are combined to form

$$u = \bar{a}U \quad \text{--- (A.1.19)}$$

where, $u = \begin{Bmatrix} u_x \\ u_y \\ u_z \end{Bmatrix}$ and $\bar{a} = \begin{Bmatrix} a_x \\ a_y \\ a_z \end{Bmatrix}$

Substituting (A.1.19) in (A.1.13), we get

$$m = \int_V \rho a_x^T a_x \, dv + \int_V \rho a_y^T a_y \, dv + \int_V \rho a_z^T a_z \, dv \qquad \text{---(A.1.20)}$$

First and second terms in equation (A.1.20) represent the rotary inertia while the third term represents the translational inertia of the element. Neglecting the rotary inertia effects, the mass matrix for the discrete element in its local coordinate system becomes:

$$m = \int_V \rho a_z^T a_z \, dv.$$

APPENDIX 2: Computer Program Documentation

COMPUTER PROGRAM DOCUMENTATION

The input to the main program includes physical dimensions, material properties and proper designation of the nodal stations used to idealize the cantilever. It generates various coordinates of the triangular elements and computes the transformation matrix used to reduce the degrees of freedom from 27 to 9. Following is the list of important subroutines:

1. Subroutine Nath computes the bending stiffness matrices of subtriangles in their respective local coordinates.

   Call and Argument List:

   CALL NATH (D1, XIISB, YIISB, XIIISB, YIIISB, POIS).

   XIISB and YIISB are the coordinate of node 2 of sub-element

   XIIISB and YIIISB are the coordinates of node 3 of the sub-element in local coordinate system

   POIS is POISSON's Ratio.

   D1 is the Bending Stiffness Matrix of the sub-element.

2. Subroutine BHAT calculates the consistent mass matrices of subtriangles in their respective local coordinates.

   Call and Argument List:

   CALL BHAT (EKB, Y2, Y3, X3, AS, AY, AMASS).

   EKB is dummy matrix of 7 x 7.

   AX and AY are dummy vectors of size 6.

   Y2 is Y local coordinate of node 2.

   X3 and Y3 are X and Y local coordinates of node 3.

   AMASS is the mass matrix for the subtriangles

3. Subroutine Asembl condenses the stiffness and mass matrices in bending of all the elements and stores them separetely as Soft and Hard respectively as column vectors, thus saving considerable core space in the computer.

   Call and Argument List:

   CALL ASEMBL (BSTIF, SOFT, MEM, NELEM, NI).

   BSTIF is 9 x 9 stiffness/mass matrix of an element to be assembled.

   SOFT is a vector of size 8001 in which the lower triangular portion of assembled matrix is stored.

   MEM is the element number.

   NELEM is twice the product of lengthwise and widthwise divisions of cantilever plate.

   NI is the matrix of size (NELEM, 3) in which node number of all the elements are stored.

4. Subroutine Power finds out the first ten highest eigenvalues, thus giving the first ten natural frequencies of the cantilever. The method used is the "Power" iterative process.

   Call and Argument List:

   CALL POWER (CKM, NR, MR, EY, EZ, ALPHA).

   CKM is the square matrix whose eigenvalues are to be determined.

   NR is the size of the matrix CKM.

   MR is the number of eigenvalues required.

   EY and EZ are dummy vectors of size NR.

ALPHA is the vector in which the eigenvalues are returned.

5. Subroutine Vector computes the corresponding ten normalized eigenmodes which represent the mode shapes of the vibrating cantilever.

Call and Argument List:

CALL VECTOR (CKM, EZ, S, NR, MR).

CKM is the matrix obtained by calling subroutine POWER.

EZ is the dummy vector of size NR.

S is the vector containing MR eigenvalues obtained from POWER subroutine.

APPENDIX 3: Computer Programmes

```
A4207,T1000,CM140000,LC1000.
RUN(S,,,,,,6000)
REDUCE.
LGO.
'         6400 END OF RECORD
      PROGRAM TST (INPUT,OUTPUT,PUNCH,TAPE5=INPUT,TAPE6=OUTPUT,TAPE7=
     1 PUNCH)
C
C        PROBLEM.
C
C        FREE VIBRATION ANALYSIS OF CANTILEVER BLADE OF CONSTANT THICKNESS
C
C        METHOD.
C
C        APPLICATION OF FINITE ELEMENT TECHNIQUE TO A FULLY COMPATIBLE
C        TRIANGULAR ELEMENT.
C
C        NOTATIONS.
C
C
C        NLD=NUMBER OF LENGTHWISE DIVISIONS.
C        NWD=NUMBER OF WIDTHWISE DIVISIONS.
C        TTW=TOTAL TWIST IN DEGREES.
C        BL=BLADE LENGTH IN INCHES.
C        BW=BLADE WIDTH IN INCHES.
C        TH=BLADE THICKNESS IN INCHES.
C        POIS=POISSONS RATIO
C        YM=YOUNGS MODULUS IN PSI.
C
C
      DIMENSION  X(3),Y(3),XG(3),YG(3),ZG(3),XP(3),YP(3),ZP(3)
      DIMENSION TLP(3,3,3),TRLP(3,9,9),TT(3,9,9),PA(9,9),PPA(9,9)
      DIMENSION A(9,9),B(9,18),C(18,9),D(18,18),E(9,18),F(9,9)
      DIMENSION ABAR(9,9),EE(18,9),EBAR(18,9),ATAR(9,27),ALPHA(10)
      DIMENSION NI(72,3),SOFT(8001),HARD(8001),AKM(126,126),EY(126)
      DIMENSION EZ(126),EKB(7,7),AX(6),AY(6),ABCM(9,9),NL(72),ML(36)
      DIMENSION ATOBI(27,9),ATOBIT(9,27),BSTIF(9,9),WORK(18)
      DIMENSION PPB(9,9),PPC(9,9),D1(9,9),D2(9,9),D3(9,9),AKBAR(27,27)
      DIMENSION SAU(9),SAV(9),SBT(9),SCT(9),SCU(9),SBV(9),TRNS(3,3,3)
C
C
C
C
      READ(5,11) NLD,NWD
      READ(5,21) TTW,BL,BW,TH,POIS
      NELEM=NLD*NWD*2
      READ(5,199) (NI(I,1),I=1,NELEM)
      READ(5,199) (NI(I,2),I=1,NELEM)
      READ(5,199) (NI(I,3),I=1,NELEM)
   11 FORMAT(2I4)
   21 FORMAT(5F12.4)
  199 FORMAT(36I2)
      TTW=0.0
      NR=(NWD+1)*NLD*3
      NW=(NR+1)*NR/2
      MR=10
      KKKK=1
      MEM=1
      DO 7771 I=1,NW
```

```
      SOFT(I)=0.0
      HARD(I)=0.0
 7771 CONTINUE
      DO 1000 NSIT=1,2
C     COMPUTATION OF NODAL COORDINATES OF DISCRETE ELEMENTS IN THE
C     DATUM SYSTEM.
      LN=NLD+1
      INTB=LN*(NWD-1)+1
      KR=0
      YNWD=NWD
      Y(1)=-BW/YNWD-BW/2.0
      DO 1000 NN=1,INTB,LN
      YNN=NN
      KR=KR+1
      IF(NSIT.EQ.2) GO TO 333
      Y(1)=Y(1)+BW/YNWD
      Y(3)=Y(1)+BW/YNWD
      Y(2)=Y(1)
      GO TO 666
  333 CONTINUE
      IF((NSIT.EQ.2).AND.(KKKK.EQ.2)) Y(1)=0.0
      IF((NSIT.EQ.2).AND.(KKKK.EQ.3)) Y(1)=BW/YNWD
      IF((NSIT.EQ.2).AND.(KKKK.EQ.4)) Y(1)=2.0*BW/YNWD
      IF((NSIT.EQ.2).AND.(KKKK.EQ.5)) Y(1)=3.0*BW/YNWD
      IF((NSIT.EQ.2).AND.(KKKK.EQ.6)) Y(1)=4.0*BW/YNWD
      Y(2)=Y(1)+BW/YNWD
      Y(3)=Y(2)+BW/YNWD
      Y(1)=Y(3)
      KKKK=KKKK+1
  666 CONTINUE
      LZ=NN-1
      LZ=LZ-KR
      DO 1000 MM=1,NLD
      XMM=MM
      XNLD=NLD
      X(1)=(XMM-1.0)*BL/XNLD
      X(2)=XMM*BL/XNLD
      X(3)=X(1)
      IF(NSIT.EQ.2)  X(3)=X(2)
      DO 111 I=1,3
      TW=TTW*X(I)*3.142/(180.*BL)
      XG(I)=X(I)
      YG(I)=Y(I)*COS(TW)
  111 ZG(I)=Y(I)*SIN(TW)
      IF(NSIT.EQ.2) GO TO 1
      XP(1)=-(2./3.)*(XG(2)-XG(1))
      XP(2)= (1./3.)*(XG(2)-XG(1))
      XP(3)=XP(2)
      YP(1)=-(1./3.)*(YG(3)-YG(2))
      YP(3)= (2./3.)*(YG(3)-YG(2))
      YP(2)=YP(1)
      IF(NSIT.EQ.1) GO TO 2
    1 XP(1)=-(1./3.)*(XG(3)-XG(1))
      XP(3)= (2./3.)*(XG(3)-XG(1))
      XP(2)=XP(1)
      YP(1)= (1./3.)*(YG(1)-YG(2))
      YP(2)=-(2./3.)*(YG(1)-YG(2))
      YP(3)=YP(1)
```

```
    2 CONTINUE
      ZP(1)=0.0
      ZP(2)=0.0
      ZP(3)=0.0
C     COMPUTATION OF NODAL COORDINATES OF SUBELEMENTS IN THE LOCAL
C     COORDINATE SYSTEM.
      A02=SQRT(XP(2)**2+YP(2)**2)
      B32=SQRT((XP(3)-XP(2))**2+(YP(3)-YP(2))**2)
      C30=SQRT(XP(3)**2+YP(3)**2)
      XIISB=(A02**2+B32**2-C30**2)/(2.0*B32)
      YIISB=SQRT(ABS(A02**2-XIISB**2))
      XIIISB=-(B32-XIISB)
      YIIISB=YIISB
      A03=SQRT(XP(3)**2+YP(3)**2)
      B13=SQRT((XP(3)-XP(1))**2+(YP(3)-YP(1))**2)
      C01=SQRT(XP(1)**2+YP(1)**2)
      XIIDB=(A03**2+B13**2-C01**2)/(2.*B13)
      YIIDB=SQRT(ABS(A03**2-XIIDB**2))
      XIIIDB=-(B13-XIIDB)
      YIIIDB=YIIDB
      A20=SQRT(XP(2)**2+YP(2)**2)
      B10=SQRT(XP(1)**2+YP(1)**2)
      C12=SQRT((XP(2)-XP(1))**2+(YP(2)-YP(1))**2)
      XIITB= (B10**2+C12**2-A20**2)/(2.*C12)
      YIITB= SQRT(ABS(B10**2-XIITB**2))
      YIIITB=YIITB
      XIIITB=-(C12-XIITB)
      CALL NATH(D1,XIISB,YIISB,XIIISB,YIIISB,POIS)
      CALL NATH(D2,XIIDB,YIIDB,XIIIDB,YIIIDB,POIS)
      CALL NATH(D3,XIITB,YIITB,XIIITB,YIIITB,POIS)
C     TO FIND AKBAR (27*27).
C     AKBAR IS THE SET OF STIFFNESS MATRICES OF THE THREE SUBTRIANGLES
C     OF THE COMPLETE ELEMENT IN THE LOCAL COORDINATE SYSTEM.
      YM=3000.0*10000.0
      Z=(YM*TH**3)/(12.*(1.-POIS**2))
      Z=1.0
      DO 38 I=1,27
      DO 38 K=1,27
   38 AKBAR(I,K)=0.
      DO 39 I=1,9
      DO 39 K=1,9
   39 AKBAR(I,K)=Z*D1(I,K)
      DO 40 I=10,18
      DO 40 K=10,18
      II=I-9
      KK=K-9
   40 AKBAR(I,K)=Z*D2(II,KK)
      DO 41 I=19,27
      DO 41 K=19,27
      II=I-18
      KK=K-18
   41 AKBAR(I,K)=Z*D3(II,KK)
      LMN=1
      J=1
      IF(NSIT.EQ.2) GO TO 26
      THETA=0.5*3.1416
      GO TO 27
   26 THETA=3.1416-ATAN((YP(3)-YP(2))/(XP(3)-XP(2)))
```

```
27    CONTINUE
      CALL TRANS(THETA,TLP,TRLP,TT,LMN,J)
      LMN=2
      J=2
      IF(NSIT.EQ.2) GO TO 28
      THETA=2.0*3.1416-ATAN((YP(3)-YP(1))/(XP(3)-XP(1)))
      GO TO 29
28    THETA=2.0*3.1416
29    CONTINUE
      CALL TRANS(THETA,TLP,TRLP,TT,LMN,J)
      LMN=3
      J=3
      IF(NSIT.EQ.2) GO TO 30
      THETA=3.1416
      GO TO 31
30    THETA=3.0*3.1416/2.0
31    CONTINUE
      CALL TRANS(THETA,TLP,TRLP,TT,LMN,J)
      NNN=1
      CALL JAG(PA,TT,XIISB,YIISB,XIIISB,YIIISB,PPA,NNN)
      NNN=2
      CALL JAG(PA,TT,XIIDB,YIIDB,XIIIDB,YIIIDB,PPB,NNN)
      NNN=3
      CALL JAG(PA,TT,XIITB,YIITB,XIIITB,YIIITB,PPC,NNN)
C     COMPUTATION OF NORMAL SLOPES AT MIDPOINTS OF INTERIOR EDGES
C     OF SUBTRIANGLES.
      XUSB=XIISB/2.
      YUSB=YIISB/2.
      THTA=ATAN(YIISB/XIISB)
      CALL SLOPE(XUSB,YUSB,SAU,THTA)
      XVSB=XIIISB/2.
      YVSB=YIIISB/2.
      THTA=3.1416-ATAN(ABS(YIIISB/XIIISB))
      CALL SLOPE(XVSB,YVSB,SAV,THTA)
      XVDB=XIIDB/2.
      YVDB=YIIDB/2.
      THTA=ATAN(YIIDB/XIIDB)
      CALL SLOPE(XVDB,YVDB,SBV,THTA)
      XTDB=XIIIDB/2.
      YTDB=YIIIDB/2.
      THTA=3.1416-ATAN(ABS(YIIIDB/XIIIDB))
      CALL SLOPE(XTDB,YTDB,SBT,THTA)
      XTTB=XIITB/2.
      YTTB=YIITB/2.
      THTA=ATAN(YIITB/XIITB)
      CALL SLOPE(XTTB,YTTB,SCT,THTA)
      XUTB=XIIITB/2.
      YUTB=YIIITB/2.
      THTA=3.1416-ATAN(ABS(YIIITB/XIIITB))
      CALL SLOPE(XUTB,YUTB,SCU,THTA)
C     MATRIX A=A11.
      DO 55 I=1,9
      DO 55 K=1,9
55    A(I,K)=0.
      DO 56 I=4,6
      DO 56 K=1,9
56    A(I,K)=PPA(I,K)
C     MATRIX B=A12.
```

```
      DO 57 I=1,9
      DO 57 K=1,18
   57 B(I,K)=0.
      DO 58 I=1,3
      DO 58 K=10,18
      II=I+3
      KK=K-9
   58 B(I,K)=PPC(II,KK)
      DO 59 I=7,9
      DO 59 K=1,9
      II=I-3
   59 B(I,K)=PPB(II,K)
C     MATRIX C=A21.
      DO 60 I=1,18
      DO 60 K=1,9
   60 C(I,K)=0.
      DO 61 K=1,9
   61 C(1,K)=-SAV(K)
      DO 62 I=2,4
      DO 62 K=1,9
      II=I-1
   62 C(I,K)=PPA(II,K)
      DO 63 I=6,8
      DO 63 K=1,9
      II=I+1
   63 C(I,K)=-PPA(II,K)
      DO 46 K=1,9
   46 C(9,K)=SAU(K)
      DO 64 I=16,18
      DO 64 K=1,9
      II=I-12
   64 C(I,K)=PPA(II,K)
C     MATRIX D=A22.
      DO 65 I=1,18
      DO 65 K=1,18
   65 D(I,K)=0.
      DO 43 K=1,9
   43 D(1,K)=SBV(K)
      DO 44 I=2,4
      DO 44 K=1,9
      II=I-1
   44 D(I,K)=-PPB(II,K)
      DO 45 K=1,9
   45 D(5,K)=-SBT(K)
      DO 66 K=10,18
      KK=K-9
   66 D(5,K)=SCT(KK)
      DO 67 I=6,8
      DO 67 K=1,9
      II=I-2
   67 D(I,K)=PPB(II,K)
      DO 68 K=10,18
      KK=K-9
   68 D(9,K)=-SCU(KK)
      DO 69 I=10,12
      DO 69 K=1,9
      II=I-3
   69 D(I,K)=-PPB(II,K)
```

```
      DO 70 I=10,12
      DO 70 K=10,18
      II=I-6
      KK=K-9
   70 D(I,K)=PPC(II,KK)
      DO 71 I=13,15
      DO 71 K=1,9
      II=I-12
   71 D(I,K)=PPB(II,K)
      DO 72 I=13,15
      DO 72 K=10,18
      II=I-12
      KK=K-9
   72 D(I,K)=-PPC(II,KK)
       DO 73 I=16,18
       DO 73 K=10,18
      II=I-9
      KK=K-9
   73 D(I,K)=-PPC(II,KK)
C     INVERTING THE MATRIX D.
      CALL MINVSE(D,18,18,1.0E-8,IERR,NL,WORK)
C     PRODUCT OF B(9*18) AND D(18*18) IS E(9*18).
      CALL PRODCT(B,D,E,9,18,18)
C     PRODUCT OF E(9,18) AND C(18,9) IS F(9,9).
      CALL PRODCT(E,C,F,9,18,9)
C     SUBTRACTION OF F(9*9) FROM A(9*9) IS ABAR(9*9).
      DO 78 I=1,9
      DO 78 K=1,9
   78 ABAR(I,K)=A(I,K)-F(I,K)
C     INVERTION OF ABAR.
      CALL MINVSE(ABAR,9,9,1.0E-8,IERR,ML,WORK)
C     PRODUCT OF -D(18,18) AND C(18,9) IS EE(18,9).
      DO 79 I=1,18
      DO 79 K=1,18
   79 D(I,K)=-D(I,K)
      CALL PRODCT(D,C,EE,18,18,9)
C     PRODUCT OF EE(18*9) AND ABAR(9*9) IS EBAR(18*9).
      CALL PRODCT(EE,ABAR,EBAR,18,9,9)
C     PUTTING ABAR(9*9) AND EBAR(18*9) AS A MATRIX OF ATOBI(27*9).
      DO 84 I=1,9
      DO 84 K=1,9
   84 ATOBI(I,K)=ABAR(I,K)
      DO 85 I=10,27
      DO 85 K=1,9
      II=I-9
   85 ATOBI(I,K)=EBAR(II,K)
C     TRANSPOSE OF ATOBI(27*9) IS ATOBIT(9*27).
      DO 86 I=1,9
      DO 86 K=1,27
   86 ATOBIT(I,K)=ATOBI(K,I)
C     STIFFNESS MATRIX BSTIF(9*9) OF THE ENTIRE TRIANGLE IJK IN BENDING
C     IS THE PRODUCT OF ATOBIT(9*27), AKBAR(27*27) AND ATOBI(27*9).
      CALL PRODCT(ATOBIT,AKBAR,ATAR,9,27,27)
      CALL PRODCT(ATAR,ATOBI,BSTIF,9,27,9)
C     SOFT IS THE SUARE SYMMETRIC CONDENSED STIFFNESS MATRIX OF THE
C     ENTIRE STRUCTURE.
      CALL ASMBL(BSTIF,SOFT,MEM,NELEM,NI)
      DO 6006 I=1,9
```

```
      DO 6006 K=1,9
      D1(I,K)=0.0
      D2(I,K)=0.0
6006  D3(I,K)=0.0
      Y2=XIISB-XIIISB
      Y3=-XIIISB
      X3=YIISB
      CALL BHAT(EKB,Y2,Y3,X3,AX,AY,D1)
      Y2=XIIDB-XIIIDB
      Y3=-XIIIDB
      X3=YIIDB
      CALL BHAT(EKB,Y2,Y3,X3,AX,AY,D2)
      Y2=XIITB-XIIITB
      Y3=-XIIITB
      X3=YIITB
      CALL BHAT(EKB,Y2,Y3,X3,AX,AY,D3)
      DO 7007 I=1,27
      DO 7007 K=1,27
7007  AKBAR(I,K)=0.0
      DO 3311 I=1,9
      DO 3311 K=1,9
3311  AKBAR(I,K)=D1(I,K)
      DO 3322 I=10,18
      DO 3322 K=10,18
      II=I-9
      KK=K-9
3322  AKBAR(I,K)=D2(II,KK)
      DO 4411 I=19,27
      DO 4411 K=19,27
      II=I-18
      KK=K-18
4411  AKBAR(I,K)=D3(II,KK)
      CALL PRODCT(ATOBIT,AKBAR,ATAR,9,27,27)
      CALL PRODCT(ATAR,ATOBI,ABCM,9,27,9)
C     ABCM IS THE MASS MATRIX OF THE ENTIRE TRIANGLE IJK IN BENDING.
C     HARD IS THE SQUARE SYMMETRIC CONDENSED MASS MATRIX OF THE
C     ENTIRE STRUCTURE.
      CALL ASMBL(ABCM,HARD,MEM,NELEM,NI)
      MEM=MEM+1
1000  CONTINUE
      CALL INVSYM (SOFT,NR,IERR)
      WRITE(6,3331) IERR
3331  FORMAT(/,10X,I3,/)
C     MULTIPLY K-INVERSE AND M. ......(SOFT*HARD)
      DO 1919 I=1,NR
      DO 1919 J=1,NR
      AKM(I,J)=0.0
      DO 1919 L=1,NR
      IF(I.GE.L) K=I*(I-1)/2+L
      IF(I.LT.L) K=L*(L-1)/2+I
      IF(L.GE.J) I1=L*(L-1)/2+J
      IF(L.LT.J) I1=J*(J-1)/2+L
1919  AKM(I,J)=AKM(I,J)+SOFT(K)*HARD(I1)
C     ALPHA(J) ARE THE FIRST TEN HIGHEST EIGEN VALUES.
      CALL POWER (AKM,NR,MR,EY,EZ,ALPHA)
      CALL VECTOR(AKM,EZ,ALPHA,NR,MR)
      DO 1920 J=1,MR
      ALPHA(J)=BL**2/SQRT(ALPHA(J))
```

```
1920  CONTINUE
      WRITE(6,459)
 459  FORMAT(//,10X,26H FIRST 10 EIGEN VALUES ARE,/)
      WRITE(6,461) (ALPHA(I),I=1,10)
      WRITE(7,462) (ALPHA(I),I=1,10)
 462  FORMAT(10X,E12.4)
 461  FORMAT(30X,E15.6)
 93   STOP
      END
```

CD TOT 0416

```
      SUBROUTINE NATH(D1,XIISB,YIISB,XIIISB,YIIISB,POIS)
      DIMENSION D1(9,9)
      DO 18 I=1,9
      DO 18 K=1,9
   18 D1(I,K)=0.
      XII=XIISB
      YII=YIISB
      XIII=XIIISB
      D1(4,4)=2.*(XII-XIII)*YII
      D1(4,6)=POIS*D1(4,4)
      D1(4,7)=3.*D1(4,4)
      D1(4,8)=(2.*POIS/3.0)*YII*(XII**2-XIII**2)
      D1(4,9)=(4.*POIS)*(XII-XIII)*(YII**2)
      D1(5,5)=(1.-POIS)*(XII-XIII)*YII
      D1(5,8)=(4.*(1.-POIS)/3.)*(XII-XIII)*(YII**2)
      D1(6,4)=D1(4,6)
      D1(6,6)=D1(4,4)
      D1(6,7)=3.*D1(4,6)
      D1(6,8)=(2./3.)*YII*(XII**2-XIII**2)
      D1(6,9)=D1(4,9)/POIS
      D1(7,4)=D1(4,7)
      D1(7,6)=D1(6,7)
      D1(7,7)=9.*D1(4,4)
      D1(7,8)=3.*D1(4,8)
      D1(7,9)=3.*D1(4,9)
      D1(8,4)=D1(4,8)
      D1(8,5)=D1(5,8)
      D1(8,6)=D1(6,8)
      D1(8,7)=D1(7,8)
      D1(8,8)=(1./3.)*YII*(XII**3-XIII**3)+2.*(XII-XIII)*
     1(1.-POIS)*YII**3
      D1(8,9)=0.5*(5.*XII**2-XIII**2)*YII**2
      D1(9,4)=D1(4,9)
      D1(9,6)=D1(6,9)
      D1(9,7)=D1(7,9)
      D1(9,8)=D1(8,9)
      D1(9,9)=9.*(XII-XIII)*YII**3
      RETURN
      END
```

CD TOT 0039

```
      SUBROUTINE TRANS(THETA,TLP,TRLP,TT,LMN,J)
      DIMENSION TLP(3,3,3),TRLP(3,9,9),TT(3,9,9)
      DO 777 I=1,3
      DO 777 K=1,3
  777 TLP(LMN,I,K)=0.0
      TLP(LMN,1,1)=1.0
      TLP(LMN,2,2)=COS(THETA)
      TLP(LMN,2,3)=SIN(THETA)
      TLP(LMN,3,2)=-SIN(THETA)
      TLP(LMN,3,3)=COS(THETA)
      DO 3 I=1,9
      DO 3 K=1,9
    3 TRLP(J,I,K)=0.0
      DO 4 I=1,3
      DO 4 K=1,3
    4 TRLP(J,I,K)=TLP(LMN,I,K)
      DO 5 I=4,6
      DO 5 K=4,6
      II=I-3
      KK=K-3
    5 TRLP(J,I,K)=TLP(LMN,II,KK)
      DO 6 I=7,9
      DO 6 K=7,9
      II=I-6
      KK=K-6
    6 TRLP(J,I,K)=TLP(LMN,II,KK)
      DO 7 I=1,9
      DO 7 K=1,9
    7 TT(J,I,K)=TRLP(J,I,K)
      RETURN
      END
```

CD TOT 0031

```
      SUBROUTINE JAG(PA,TT,XIISB,YIISB,XIIISB,YIIISB,PPA,NNN)
      DIMENSION PA(9,9),TT(3,9,9),PPA(9,9)
      DO 8 I=1,9
      DO 8 K=1,9
8     PA(I,K)=0.0
      PA(1,1)=1.0
      PA(2,3)=1.0
      PA(3,2)=-1.0
      PA(4,1)=1.0
      PA(4,2)=XIISB
      PA(4,3)=YIISB
      PA(4,4)=PA(4,2)**2
      PA(4,5)=PA(4,2)*PA(4,3)
      PA(4,6)=PA(4,3)**2
      PA(4,7)=PA(4,2)**3
      PA(4,8)=PA(4,2)*PA(4,3)**2
      PA(4,9)=PA(4,3)**3
      PA(5,3)=1.0
      PA(5,5)=PA(4,2)
      PA(5,6)=2.*PA(4,3)
      PA(5,8)=2.*PA(4,2)*PA(4,3)
      PA(5,9)=3.*PA(4,3)**2
      PA(6,2)=-1.0
      PA(6,4)=-2.*PA(4,2)
      PA(6,5)=-1.*PA(4,3)
      PA(6,7)=-3.*PA(4,2)**2
      PA(6,8)=-1.*PA(4,3)**2
      PA(7,1)=1.0
      PA(7,2)=XIIISB
      PA(7,3)=YIIISB
      PA(7,4)=PA(7,2)**2
      PA(7,5)=PA(7,2)*PA(7,3)
      PA(7,6)=PA(7,3)**2
      PA(7,7)=PA(7,2)**3
      PA(7,8)=PA(7,2)*PA(7,3)**2
      PA(7,9)=PA(7,3)**3
      PA(8,3)=1.0
      PA(8,5)=PA(7,2)
      PA(8,6)=2.*PA(7,3)
      PA(8,8)=2.*PA(7,2)*PA(7,3)
      PA(8,9)=3.*PA(7,3)**2
      PA(9,2)=-1.
      PA(9,4)=-2.*PA(7,2)
      PA(9,5)=-1.*PA(7,3)
      PA(9,7)=-3.*PA(7,2)**2
      PA(9,8)=-1.*PA(7,3)**2
      DO 9 I=1,9
      DO 9 K=1,9
      SUM=0.
      DO 10 L=1,9
10    SUM=SUM+TT(NNN,I,L)*PA(L,K)
9     PPA(I,K)=SUM
      RETURN
      END
```

CD TOT 0054

```
      SUBROUTINE SLOPE(XUSB,YUSB,SAU,THTA)
      DIMENSION SAU(9)
      SAU(1)=0.0
      SAU(2)=-SIN(THTA)
      SAU(3)=COS(THTA)
      SAU(4)=-2.0*XUSB*SIN(THTA)
      SAU(5)=-YUSB*SIN(THTA)+XUSB*COS(THTA)
      SAU(6)=2.*YUSB*COS(THTA)
      SAU(7)=-3.0*SIN(THTA)*XUSB**2
      SAU(8)=2.0*XUSB*YUSB*COS(THTA)-SIN(THTA)*YUSB**2
      SAU(9)=3.*COS(THTA)*YUSB**2
      RETURN
       END
```

```
      SUBROUTINE PRODCT(AB,BC,AC,M,N,L)
      DIMENSION AB(M,N),BC(N,L),AC(M,L)
      DO 1 LL=1,L
      DO 1 MM=1,M
      AC(MM,LL)=0.0
      DO 1 NN=1,N
    1 AC(MM,LL)=AC(MM,LL)+AB(MM,NN)*BC(NN,LL)
      RETURN
      END
```

```
      SUBROUTINE ASMBL(BSTIF,SOFT,MEM,NELEM,NI)
      DIMENSION BSTIF(9,9),NI(72,3),SOFT(8001)
      DO 99 I=1,3
      LL=NI(MEM,I)
      IF(LL.EQ.0) GO TO 99
      DO 98 J=1,3
      MM=NI(MEM,J)
      IF(MM.EQ.0) GO TO 98
      II=(I-1)*3
      JJ=(J-1)*3
      M=(LL-1)*3
      N=(MM-1)*3
      DO 96 IM=1,3
      DO 96 JM=1,3
      IN=IM+II
      JN=JM+JJ
      IL=IM+M
      JL=JM+N
      IF(JL.GT.IL) GO TO 96
      ILN=(IL*(IL-1)/2)+JL
      SOFT(ILN)=SOFT(ILN)+BSTIF(IN,JN)
   96 CONTINUE
   98 CONTINUE
   99 CONTINUE
      RETURN
      END
```

CD TOT 0056

```
      SUBROUTINE BHAT(EKB,Y2,Y3,X3,AX,AY,AMASS)
      DIMENSION EKB(7,7),AX(6),AY(6),AMASS(9,9)
      AX(1)=0.9324695142
      AX(2)=-AX(1)
      AX(3)=0.6612093864
      AX(4)=-AX(3)
      AX(5)=0.2386191860
      AX(6)=-AX(5)
      AY(1)=0.1713244923
      AY(2)=AY(1)
      AY(3)=0.3607615730
      AY(4)=AY(3)
      AY(5)=0.4679139345
      AY(6)=AY(5)
      DO 1 I=1,7
      DO 1 J=1,7
      M=I-1
      N=J-1
      AM=M
      AN=N
      SUM=0.0
      DO 2 K=1,6
      SS=0.5*AX(K)+0.5
      FF=(1.0-SS)**M*((1.0-SS)*Y3+SS*Y2)**N
    2 SUM=SUM+AY(K)*FF*0.5
      EKB(I,J)= SUM*X3**(M+1)*Y2/(AM+AN+2.0)
    1 CONTINUE
      AMASS(1,1)=EKB(1,1)
      AMASS(2,1)=EKB(1,2)-Y3*EKB(1,1)
      AMASS(3,1)=X3*EKB(1,1)-EKB(2,1)
      AMASS(4,1)=EKB(1,3)-2.*Y3*EKB(1,2)+Y3**2*EKB(1,1)
      AMASS(5,1)=X3*EKB(1,2)-EKB(2,2)-Y3*X3*EKB(1,1)+Y3*EKB(2,1)
      AMASS(6,1)=X3**2*EKB(1,1)-2.*X3*EKB(2,1)+EKB(3,1)
      AMASS(7,1)=EKB(1,4)-3.*Y3*EKB(1,3)+3.*Y3**2*EKB(1,2)-Y3**3*
     1 EKB(1,1)
      AMASS(8,1)=X3**2*EKB(1,2)-2.*X3*EKB(2,2)+EKB(3,2)-Y3*X3**2*EKB(
     1 1,1)+2.*Y3*X3*EKB(2,1)-Y3*EKB(3,1)
      AMASS(9,1)=X3**3*EKB(1,1)-3.*X3**2*EKB(2,1)+3.*X3*EKB(3,1)
     1 -EKB(4,1)
      AMASS(2,2)=AMASS(4,1)
      AMASS(3,2)=AMASS(5,1)
      AMASS(4,2)=AMASS(7,1)
      AMASS(5,2)=X3*EKB(1,3)-2.*Y3*X3*EKB(1,2)+Y3**2*X3*EKB(1,1)-
     1 EKB(2,3)+2.*Y3*EKB(2,2)-Y3**2*EKB(2,1)
      AMASS(6,2)=AMASS(8,1)
      AMASS(7,2)=EKB(1,5)-4.*Y3*EKB(1,4)-4.*Y3**3*EKB(1,2)+6.*Y3**2*
     1 EKB(1,3)+Y3**4*EKB(1,1)
      AMASS(8,2)=X3**2*EKB(1,3)-2.*X3*EKB(2,3)+EKB(3,3)-2.*Y3*X3**2*
     1 EKB(1,2)+4.*Y3*X3*EKB(2,2)+Y3**2*EKB(3,1)
     1 -2.0*Y3*EKB(3,2)+X3**2*Y3**2*EKB(1,1)-2.*Y3**2*X3*EKB(2,1)
      AMASS(9,2)=X3**3*EKB(1,2)-3.0*X3**2*EKB(2,2)+3.0*X3*EKB(3,2)
     1 -EKB(4,2)-Y3*X3**3*EKB(1,1)+3.0*Y3*X3**2*EKB(2,1)-3.0*Y3*X3*EKB(
     1 3,1)+Y3*EKB(4,1)
      AMASS(3,3)=AMASS(6,1)
      AMASS(4,3)=AMASS(5,2)
      AMASS(5,3)=AMASS(6,2)
      AMASS(6,3)=AMASS(9,1)
      AMASS(7,3)=X3*EKB(1,4)-3.*Y3*X3*EKB(1,3)+3.*Y3**2*X3*EKB(1,2)
     1 -Y3**3*X3*EKB(1,1)-EKB(2,4)+3.*Y3*EKB(2,3)-3.*Y3**2*EKB(2,2)+
```

```
     1 Y3**3*EKB(2,1)
       AMASS(8,3)=AMASS(9,2)
       AMASS(9,3)=X3**4*EKB(1,1)-4.*X3**3*EKB(2,1)-4.*X3*EKB(4,1)
     1 +6.*X3**2*EKB(3,1)+EKB(5,1)
       AMASS(4,4)=AMASS(7,2)
       AMASS(5,4)=AMASS(7,3)
       AMASS(6,4)=AMASS(8,2)
       AMASS(7,4)=EKB(1,6)-5.*Y3*EKB(1,5)+5.*Y3**4*EKB(1,2)-10.*Y3**3*
     1 EKB(1,3)+10.*Y3**2*EKB(1,4)-Y3**5*EKB(1,1)
       AMASS(8,4)=X3**2*EKB(1,4)-3.*Y3*X3**2*EKB(1,3)+3.*Y3**2*X3**2*
     1 EKB(1,2)-Y3**3*X3**2*EKB(1,1)-2.*X3*EKB(2,4)+6.*Y3*X3*EKB(2,3)
     1 -6.*Y3**2*X3*EKB(2,2)+2.*Y3**3*X3*EKB(2,1)+EKB(3,4)-3.*Y3*EKB(
     1 3,3)+3.*Y3**2*EKB(3,2)-Y3**3*EKB(3,1)
       AMASS(9,4)=X3**3*EKB(1,3)-3.*X3**2*EKB(2,3)+3.*X3*EKB(3,3)-
     1 EKB(4,3)-2.*Y3*X3**3*EKB(1,2)+6.*Y3*X3**2*EKB(2,2)-6.*Y3*X3*EKB(
     1 3,2)+2.*Y3*EKB(4,2)+Y3**2*X3**3*EKB(1,1)-3.*Y3**2*X3**2*EKB(2,1)
     1 +3.*Y3**2*X3*EKB(3,1)-Y3**2*EKB(4,1)
       AMASS(5,5)=AMASS(6,4)
       AMASS(6,5)=AMASS(8,3)
       AMASS(7,5)=X3*EKB(1,5)-4.*Y3*X3*EKB(1,4)-4.*Y3**3*X3*EKB(1,2)
     1 +6.*Y3**2*X3*EKB(1,3)+Y3**4*X3*EKB(1,1)-EKB(2,5)+4.*Y3*EKB(2,4)
     1 +4.*Y3**3*EKB(2,2)-6.*Y3**2*EKB(2,3)-Y3**4*EKB(2,1)
       AMASS(8,5)=AMASS(9,4)
       AMASS(9,5)=X3**4*EKB(1,2)-4.*X3**3*EKB(2,2)-4.*X3*EKB(4,2)+6.*
     1 X3**2*EKB(3,2)+EKB(5,2)-Y3*X3**4*EKB(1,1)+4.*Y3*X3**3*EKB(2,1)+
     1 4.*Y3*X3*EKB(4,1)-6.*Y3*X3**2*EKB(3,1)-Y3*EKB(5,1)
       AMASS(6,6)=AMASS(9,3)
       AMASS(7,6)=AMASS(8,4)
       AMASS(8,6)=AMASS(9,5)
       AMASS(9,6)=X3**5*EKB(1,1)-5.*X3**4*EKB(2,1)+5.*X3*EKB(5,1)-
     1 10.*X3**2*EKB(4,1)+10.*X3**3*EKB(3,1)-EKB(6,1)
       AMASS(7,7)=EKB(1,7)-6.*Y3*EKB(1,6)-6.*Y3**5*EKB(1,2)+15.*
     1 Y3**4*EKB(1,3)+15.*Y3**2*EKB(1,5)-20.*Y3**3*EKB(1,4)+Y3**6*EKB
     1 (1,1)
       AMASS(8,7)=X3**2*EKB(1,5)-4.*Y3*X3**2*EKB(1,4)-4.*Y3**3*X3**2*EKB
     1 (1,2)+6.*Y3**2*X3**2*EKB(1,3)+Y3**4*X3**2*EKB(1,1)-2.*X3*EKB(2,5)
     1 +8.*Y3*X3*EKB(2,4)+8.*Y3**3*X3*EKB(2,2)-12.*Y3**2*X3*EKB(2,3)
     1 -2.*Y3**4*X3*EKB(2,1)+EKB(3,5)-4.*Y3*EKB(3,4)-4.*Y3**3*EKB(3,2)
     1 +6.*Y3**2*EKB(3,3)+Y3**4*EKB(3,1)
       AMASS(9,7)=X3**3*EKB(1,4)-3.*X3**2*EKB(2,4)+3.*X3*EKB(3,4)-EKB(
     1 4,4)-3.*Y3*X3**3*EKB(1,3)+9.*Y3*X3**2*EKB(2,3)-9.*Y3*X3*
     1 EKB(3,3)+3.*Y3*EKB(4,3)+3.*Y3**2*X3**3*EKB(1,2)-9.*Y3**2*X3**2*
     1 EKB(2,2)+9.*Y3**2*X3*EKB(3,2)-3.*Y3**2*EKB(4,2)-Y3**3*X3**3*
     1 EKB(1,1)+3.*Y3**3*X3**2*EKB(2,1)-3.*Y3**3*X3*EKB(3,1)+
     1 Y3**3*EKB(4,1)
       AMASS(8,8)=X3**4*EKB(1,3)-4.*X3**3*EKB(2,3)-4.*X3*EKB(4,3)+
     1 6.*X3**2*EKB(3,3)+EKB(5,3)-2.*Y3*X3**4*EKB(1,2)+8.*Y3*X3**3*EKB(
     1 2,2)+8.*Y3*X3*EKB(4,2)-12.*Y3*X3**2*EKB(3,2)-2.*Y3*EKB(5,2)+
     1 Y3**2*X3**4*EKB(1,1)-4.*Y3**2*X3**3*EKB(2,1)-4.*Y3**2*X3*EKB(4,1)
     1 +6.*Y3**2*X3**2*EKB(3,1)+Y3**2*EKB(5,1)
       AMASS(9,8)=X3**5*EKB(1,2)-5.*X3**4*EKB(2,2)+5.*X3*EKB(5,2)-
     1 10.*X3**2*EKB(4,2)+10.*X3**3*EKB(3,2)-EKB(6,2)-Y3*X3**5*EKB(1,1)+
     1 5.*Y3*X3**4*EKB(2,1)-5.*Y3*X3*EKB(5,1)+10.*Y3*X3**2*EKB(4,1)-
     1 10.*Y3*X3**3*EKB(3,1)+Y3*EKB(6,1)
       AMASS(9,9)=X3**6*EKB(1,1)-6.*X3**5*EKB(2,1)-6.*X3*EKB(6,1)+
     1 15.*X3**2*EKB(5,1)+15.*X3**4*EKB(3,1)-20.*X3**3*EKB(4,1)
     1 +EKB(7,1)
```

```
      K=1
      DO 3 I=1,8
      K=K+1
      DO 3 J=K,9
 3    AMASS(I,J)=AMASS(J,I)
      RHOTEE=0.28*TH/386.0
      RHOTEE=1.0
      DO 4 I=1,9
      DO 4 J=1,9
      AMASS(I,J)=RHOTEE*AMASS(I,J)
 4    CONTINUE
      RETURN
      END
```

CD TOT 0129

```
      SUBROUTINE POWER (CKM,NR,MR,EY,EZ,ALPHA)
      DIMENSION EY(NR),EZ(NR),CKM(NR,NR),ALPHA(MR)
      NN=NR+1
      DO 14 L=1,MR
      NN=NN-1
      DO 1 I=1,NN
      EY(I)=1.0
    1 CONTINUE
      BETA=1.0
    5 DO 2 I=1,NN
      EZ(I)=0.0
      DO 2 K=1,NN
    2 EZ(I)=EZ(I)+CKM(I,K)*EY(K)
      ALPHA(L)=0.0
      DO 3 I=1,NN
      IF(ABS(EZ(I)).GT.ALPHA(L)) ALPHA(L)=ABS(EZ(I))
    3 CONTINUE
      IF(ABS((ALPHA(L)-BETA)/BETA).LT.1.E-4) GO TO 6
      BETA=ALPHA(L)
      DO 4 I=1,NN
      EY(I)=EZ(I)/ALPHA(L)
    4 CONTINUE
      GO TO 5
    6 CONTINUE
      BETA=EY(1)
      DO 9 I=1,NN
      EY(I)=EY(I)/BETA
    9 CONTINUE
      DO 12 J=1,NN
      EZ(J)=CKM(1,J)
   12 CONTINUE
      DO 10 I=1,NN
      DO 10 J=1,NN
      K=NN+1-I
      CKM(K,J)=CKM(K,J)-EY(K)*CKM(1,J)
   10 CONTINUE
      DO 11 I=2,NN
      DO 11 J=2,NN
      M=I-1
      N=J-1
   11 CKM(M,N)=CKM(I,J)
      DO 13 J=2,NN
      I=J-1
   13 CKM(NN,I)=EZ(J)
      DO 14 I=1,NN
      CKM(I,NN)=EY(I)
   14 CONTINUE
      RETURN
      END
```

CD TOT 0049

```
      SUBROUTINE VECTOR(CKM,EZ,S,NR,MR)
      DIMENSION CKM(NR,NR),EZ(NR),S(MR)
      DO 8 M=1,MR
      N=MR-M
      MM=N+1
      L=NR-N
      DO 2 I=1,L
      EZ(I)=CKM(I,L)
    2 CONTINUE
      IF(N.EQ.0) GO TO 7
    6 L=NR-N
      LL=L+1
      CC=0.0
      NN=N+1
      DO 3 I=1,L
      CC=CC+EZ(I)*CKM(LL,I)
    3 CONTINUE
      CC=(S(MM)-S(N))/CC
      DO 4 I=1,L
      EZ(I)=EZ(I)*CC
    4 CONTINUE
      DO 5 I=1,L
      J=L+2-I
      NN=J-1
    5 EZ(J)=EZ(NN)+CKM(J,LL)
      EZ(1)=CKM(1,LL)
      N=N-1
      IF(N.GT.0) GO TO 6
    7 CC=ABS(EZ(1))
      DO 9 I=2,NR
      IF(ABS(EZ(I)).GT.CC) CC=ABS(EZ(I))
    9 CONTINUE
      DO 10 I=1,NR
      EZ(I)=EZ(I)/CC
   10 CONTINUE
      WRITE(6,50) MM
   50 FORMAT(/,5X,16HEIGEN VECTOR NO.,1X,I2,1X,2HIS,/)
      WRITE(7,51) MM
   51 FORMAT(5X,16HEIGEN VECTOR NO.,1X,I2,1X,2HIS,)
      WRITE(6,1) (EZ(I),I=1,NR)
    8 WRITE(7,15) (EZ(I),I=1,NR)
    1 FORMAT(5(5X,6E16.6,/))
   15 FORMAT(5X,6E12.4)
      RETURN
      END
```

CD TOT   0045

APPENDIX 4: List of Equipment

List of Equipment

Micrometer proximity transducer (type DISA 51D11)

Oscillator (Type DISA 51E02 462)

Reactance converter (Type DISA 51E01)

Electromagnet (Type Leybold SC-1004)

Oscilloscope (Type Tektronik 564)

6"x2"x1/16" thick M.S.plate with and without pretwist

Frequency Generator (0-11KcS)

Goodmans Vibration Shaker (Model 790/419)

Vibration Shaker Amplifier

CDC 6400 Digital Computer